Marine and Petroleum Geology 126 (2021) 104803

Contents lists available at ScienceDirect

Marine and Petroleum Geology

journal homepage: www.elsevier.com/locate/marpetgeo

Research paper

Depositional architecture and evolution of basin-floor fan systems since the Late Miocene in the Northwest Sub-Basin, South China Sea

Hui Chen [a,c], Dorrik A.V. Stow [b,d,**], Xinong Xie [b,c,*], Jianye Ren [b], Kainan Mao [e], Ya Gao [b], Beichen Chen [b], Wenyan Zhang [f], Thomas Vandorpe [g,h], David Van Rooij [h]

[a] School of Marine Sciences, Sun Yat-sen University, Zhuhai, Guangdong, 519082, China
[b] Hubei Key Laboratory of Marine Geological Resources, China University of Geosciences (CUG), Wuhan, Hubei, 430074, PR China
[c] Southern Marine Science and Engineering Guangdong Laboratory (Zhuhai), Zhuhai, Guangdong, 519000, China
[d] Institute of Geo-Energy Engineering, Heriot-Watt University, Edinburgh, EH14 4AS, Scotland, UK
[e] College of Resource and Environmental Engineering, Guizhou Institute of Technology, Guiyang, Guizhou, 550003, PR China
[f] Institute of Coastal Research, Helmholtz-Zentrum Geesthacht, 21502, Geesthacht, Germany
[g] Flanders Marine Institute, Wandelaarkaai 7, 8400, Oostende, Belgium
[h] Ghent University, Department of Geology, Renard Centre of Marine Geology, Krijgslaan 281 s8, B-9000, Ghent, Belgium

ARTICLE INFO

Keywords:
Basin-floor submarine fans
Architectural elements
Seismic facies
Northwest Sub-Basin
South China Sea

ABSTRACT

The sediment budget of the Northwest Sub-basin, South China Sea since the Late Miocene (11.6 Ma, average thickness > 1000 m) accounts for more than two-thirds of the total infill since the initial ocean spreading of the sub-basin (32 Ma). The sediment sources and architectural pattern of these deposits, however, are poorly known. Using high-resolution 2D reflection seismic data with age constraint from IODP boreholes, we have documented two interdigitating basin-floor fan systems that developed since the Late Miocene. These were fed by two of the largest deep-water canyon systems worldwide, from the west (the Central Canyon/Xisha Trough) and the northeast (the Pearl River Canyon), as well as from smaller headless canyons and gullies across the surrounding slopes. Based on careful analysis of seismic facies, their geometry and occurrence, we identify the principal deep-water architectural elements, including the multi-scale channels, channel-levee complexes, lobes, sheets and drapes, mass-transport deposits, volcanic intrusions, turbidity-current sediment-wave fields, and a contourite drift/terrace.

Tentative reconstructions show that the development of these Late Miocene-Quaternary basin-floor fan systems was dominated by changes of sediment supply. The Xisha fan reached its largest extent during the Late Miocene, while the Pearl River fan was most active during the Late Miocene to Quaternary. During the Late Miocene, both the conduits of the Central Canyon and the Pearl River Canyon were active with abundant sediment supply, generating the two incipient fan systems. Sediment supply from the west via the Central Canyon persisted throughout the Late Miocene, being coarser-grained than that of the Pearl River fan. With the demise of the Central Canyon during the Pliocene and consequent sharp decrease in sediment supply, the Xisha fan size reduced significantly. By contrast, supply of mud-rich sediments from the Pearl River and northern slope increased through the Pliocene and into the Quaternary, leading to the modern sedimentary pattern of interdigitating basin-floor fans. Insights into the evolution of sediment supply and fan development through time derived in this study contribute to a better understanding of how source to sink systems feed marginal oceanic basins such as the South China Sea.

1. Introduction

Submarine fans are distinctive constructional features, comprising turbidites and associated facies, which develop in deep water seawards of a major sediment source, such as a river, delta, alluvial fan or glacial tongue. In many cases, sediment is transported via turbidity currents

* Corresponding author. Hubei Key Laboratory of Marine Geological Resources, China University of Geosciences (CUG), Wuhan, 430074, PR China.
** Corresponding author. Institute of Geo-Energy Engineering, Heriot-Watt University, Edinburgh, EH14 4AS, Scotland, UK.
E-mail addresses: d.stow@hw.ac.uk (D.A.V. Stow), xnxie@cug.edu.cn (X. Xie).

https://doi.org/10.1016/j.marpetgeo.2020.104803
Received 7 December 2019; Received in revised form 30 September 2020; Accepted 2 November 2020
Available online 6 January 2021

through a major canyon-channel downslope to construct a submarine fan in a base-of-slope or basin-plain setting, i.e., slope fans and basin-floor fans (e.g., Mutti, 1985). Development of slope fans is associated with a change in bathymetric gradient between the base of the contemporaneous continental slope and upper portion of the basin floor (van Wagoner et al., 1988; Browne et al., 2005). Ponded fans develop due to confined sediment gravity flows where the slope has bowl-shaped and completely closed basins (Badalini et al., 2000; Pirmez et al., 2000; Prather, 2003; Madof et al., 2009; Gamberi and Rovere, 2011). In areas characterized by a normal downslope gradient decrease, turbidity currents freely spread in the basin plain and develop basin-floor fans in a lobate form with broad spatial extent (van Wagoner et al., 1988; King et al., 1994; Johnson et al., 2001; Saller et al., 2004; Yang and Kim, 2014). Mass-transport processes further add to fan construction through slope collapse and downslope movement (e.g., (Piper et al., 1997)). Prolonged sediment supply, over periods of 10^6 y to 10^7 y, allows the build-up of fan thicknesses from <1 km to over 15 km, and prolongation of the fan radius (or length) from 1 km to 3000 km. Since the 1970s, a number of conceptual models explaining the construction of submarine fan systems have been developed (Normark, 1970; Mutti and Ricci Lucchi, 1972; Walker, 1978; Nilsen, 1980; Stow, 1981, 1985a; Mutti and Normark, 1987; Shanmugam et al., 1988; Normark et al., 1993; Reading and Richards, 1994), along with numerous case studies of fans, modern and ancient, throughout the world (Bouma et al., 1985; Shanmugam et al., 1988; Stow, 1992; Pickering et al., 1995; Stow et al., 1996; Stow and Johansson, 2000; Piper and Normark, 2001; Mulder 2011; Pickering and Hiscott, 2015; Hessler and Fildani, 2019).

In general, the fundamental development and evolution of submarine fans is controlled by regional tectonics, sea-level fluctuations, climate, and the availability of long-term sediment supply. In addition, the interaction of downslope processes with oceanographic processes (e.g. bottom currents, internal tides), local tectonic effects (e.g. basin constriction) and seafloor morphology can be very significant (Stow, 1985a; Posamentier et al., 1988; Stow and Mayall, 2000; Piper and Normark, 2001; Normark et al., 2006; Shanmugam, 2006; Kolla, 2007; Wynn et al., 2007; Knudson and Hendy, 2009; Mulder and Etienne, 2010). As a consequence, submarine fans record long- and short-term climatic, tectonic and oceanographic changes (e.g., Bouma, 2001; Schwenk et al., 2005; Kneller et al., 2009).

Due to their importance for hydrocarbon exploration and reservoir entrapment, the sedimentary architecture of submarine fans as well as the depositional and transport processes within turbidite systems, have received much scientific attention over the last decades (Weimer et al., 2000; Shanmugam, 2006; Deptuck and Sylvester, 2018). In particular, extensive work exists on the sedimentary and seismic characterization of the specific architectural elements that make up these fan systems. These include channel complexes, channel-levee complexes, channel-lobe transitions, lobes and mass-transport deposits (MTDs). It is very important to be able to distinguish between these different elements in the subsurface in order to derive a comprehensive understanding of their formation, development and attribute dimensions (Weimer, 1989; Shanmugam and Moiola, 1991; Reading and Richards, 1994; Clark and Pickering, 1996; Gervais et al., 2006; Deptuck et al., 2008; Mulder and Etienne, 2010).

This paper focuses on the architectural elements, sequence stratigraphy and evolution of submarine fan systems that may have developed along the northern continental margin of the South China Sea (SCS) since the Late Miocene (from 11.6 Ma). In particular, two possible overlapping basin-floor fan systems are examined through seismic profiles in this paper. We suggest they have spread into the Northwest Sub-Basin (NWSB) of the SCS and were majorly fed from the Central Canyon/Xisha Trough and from the Pearl River Canyon. Their principal architectural elements, morphology, dimensions and spatial distribution are identified and documented here, based on seismic facies interpretation of 2D seismic reflection data, which have not previously been comprehensively studied. This enables us to assess the possible evolution of sediment supply and fan development through time, as well as to consider the implication for regional tectonic and oceanographic history.

2. Regional setting

2.1. Geological background

The SCS is a large (about 2.32×10^6 km^2) semi-enclosed marginal sea separating the Asian continent from the Pacific Ocean. It has a broad shelf (up to ~400 km wide) and slope adjoining the continent in the north and extends into an even larger shelf area (up to 1000 km wide), including the Sunda Shelf and Gulf of Thailand in the SW (Fig. 1). The slope is quite varied and morphologically irregular, with gradients varying from a gentle 1° to an over-steepened slope in excess of 7°. The abyssal basin floor is over 3000 m deep and ranges down to a maximum depth of ~4600 m, with a number of bathymetric highs, banks and seamounts.

The SCS abyssal basin areas have been subdivided into the Northwest, Central/East and Southwest sub-basins (Sun et al., 2009; Wang and Li, 2009a). The NWSB (113°E to 117°E, 17°N to 19°N) is bounded by the Yinggehai-Qiongdongnan Basin to the west, by the Pearl River Mouth Basin to the north, by the Zhongsha Uplifts to the south, and by the Central Sub-Basin to the southeast (Fig. 1b). The abyssal plain of the NWSB lies at an average water depth in excess of 3000 m and covers an area of over 40000 km^2. The NWSB experienced an initial spreading stage with intense faulting from about 32 to 23 Ma (Sun et al., 2006; Ding et al., 2009) (Figs. 1b and 2a). Subsequently, a subsidence stage occurred from about 23 Ma onwards (Ru and Pigott, 1986; Chen et al., 1994; Li et al., 2009; 2009b; Zhu et al., 2009; Kang et al., 2014) (Fig. 3). From about 23 to 11.6 Ma, the NWSB was a full deep-water environment, but received limited sediment input, amounting to little over 400 ms Two Way Travel Time (TWT) for the average thickness (Yin et al., 2018; Wu et al., 2018) (Fig. 4). By contrast, from about 11.6 Ma onwards, a relatively thick deep-water succession developed (Su et al., 2009, 2014; Xie et al., 2011; He et al., 2013; Yin et al., 2018). Some researchers suggested that these sediments are submarine fan deposits filling almost half the basin sequence (e.g., Liu et al., 2012; Li et al., 2017) (Figs. 3 and 4). In this region, the mainly flat seafloor is punctuated by several groups of seamounts (*s.A/s.A′*, *s.B* and *s.C/s.C′*) as shown in Fig. 2b. These seamounts are made up of scattered mafic volcanic rocks, and are believed to have formed during the post-spreading stage (Yin et al., 2018), which lasted from the Late Miocene onwards and peaked during the Late Pliocene-Pleistocene (Mao et al., 2015) (Fig. 3).

The northern SCS margin experienced reginal tectonics of the Baiyun Event (~23 Ma), the collision between Palawan and Luzon (~20–~15.5 Ma), the Dongsha Event/collision between North Palawan Block and Luzon Arc (~11.6 Ma), and the Bashi Channel formation/Rise Taiwan/collision between Luzon Arc and Eurasian plate (~5.3 Ma) (Taylor and Hayes 1983; Leloup et al., 1995; Yan et al., 2006). The Pearl River and Red River systems are suggested to act as the primary sources of sediments filling the shelf/slope-centred sedimentary basins (e.g., the Pearl River Mouth Basin and Yinggehai-Qiongdongnan Basin) over the northern SCS margin (Figs. 1 and 3). The sediment that travelled further downslope, via the Pearl River Mouth Canyon and the Central Canyon Xisha Trough, led to the development of submarine fan systems (Pang et al., 2007; Su et al., 2009, 2011, 2014; Gong et al., 2011; He et al., 2011; Ding et al., 2013; Chen et al., 2015; Li et al., 2017).

The Pearl River has served as the predominant sediment supplier draining the hinterland in the Pearl River Mouth Basin since the Early Miocene and gradually developed into the present setting, enlarging its influence in the northern SCS (Shao et al., 2019). Within the Pearl River Mouth Basin, the paleo-Pearl River delta and associated Pearl River Canyon (Fig. 1b) developed since the Early Miocene. The correlative Early-Middle Miocene deep-water fan deposits beneath the Baiyun slope

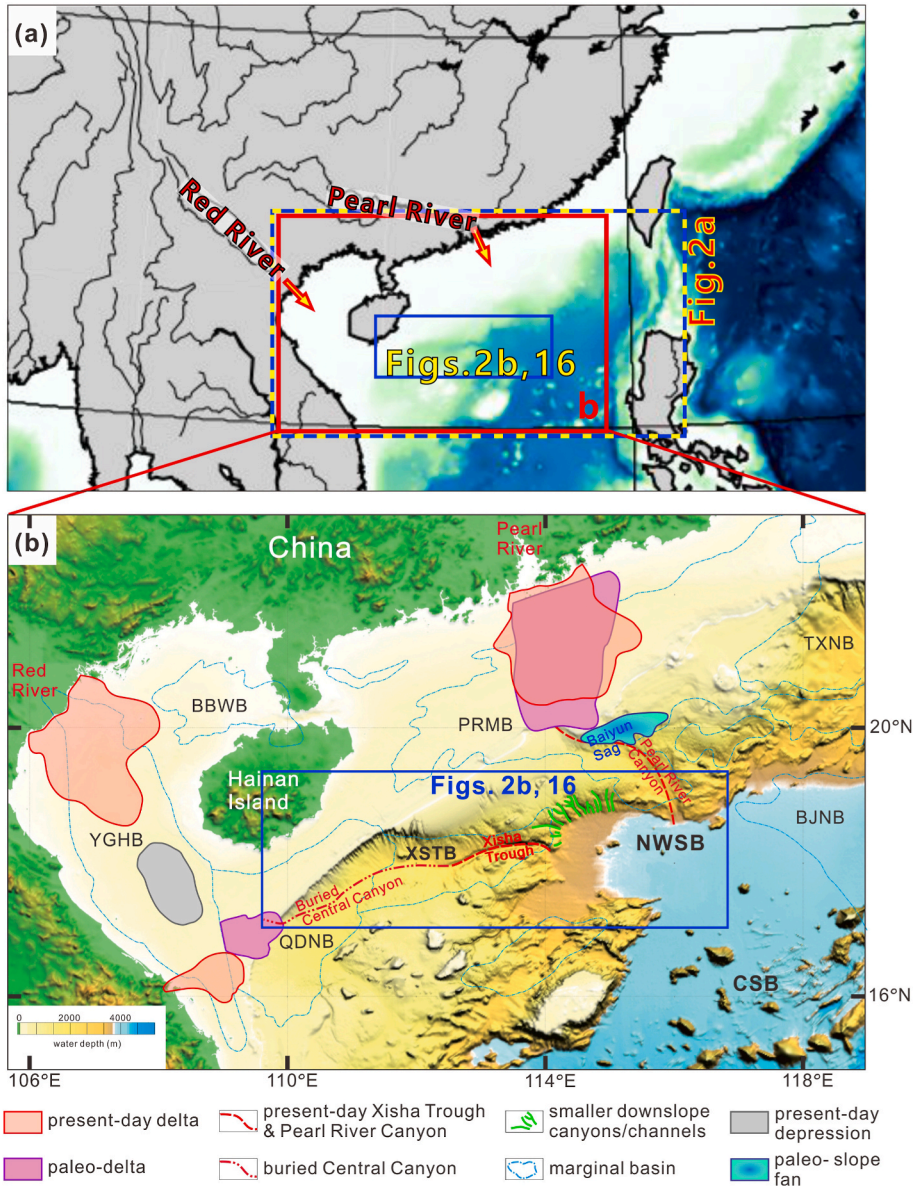

Fig. 1. A. The regional geography and principal rivers (the Red River and the Pearl River) surrounding the South China Sea (SCS) (extrapolated from GEBCO gridded bathymetry data); The red box is an inset of Fig. 1B; The dashed yellow and blue box is an inset of Fig. 2A; The blue box is an inset of Figs. 2B and 16; **B**. Bathymetric map of the mid-northern part of the SCS with the locations and names of the sedimentary basins (published by Guangzhou Marine Geological Survey and modified from Chen et al., 2015; Chen et al., 2019); Red dashed lines indicate submarine canyons; NWSB=Northwest Sub-Basin; CSB=Central Sub-Basin; BBWB=Beibuwan Basin; YGHB=Ying gehai Basin; QDNB = Qiongdongnan Basin; XSTB = Xisha Trough Basin; PRMB=Pearl River Mouth Basin; TXNB = Taixinan Basin; BJNB=Bijianan Basin; The blue box is an inset of Figs. 2B and 16. (For interpretation of the references to colour in this figure legend, the reader is referred to the Web version of this article.)

have been proven to yield good-quality hydrocarbon reservoirs (Pang et al., 2007; Zheng et al., 2007; Liu et al., 2011; Xu et al., 2013). Gigantic volume of Quaternary MTDs (over 600 km^3) have been imaged on seismic data transporting through the Pearl River Canyon and northern slope region into the NSWB (Sun et al., 2017; 2018a, b).

The modern Red River system (incl. the Red River delta that extends through the Hanoi sag) is one of the largest drainage systems and sources of sediments for the Quaternary Yinggehai Basin (van Hoang et al., 2009; Wang et al., 2019) (Fig. 1b). During the middle Miocene–Quaternary provenance evolution, Central Vietnam and Hainan Island are suggested as potential source areas in addition to the Red River system (Jiang et al., 2015; Cao et al., 2015; Wang et al., 2019). During the Middle Miocene, the Red River system might feed massive sediments to the Yinggehai basin, while sediments from Hainan Island and Central Vietnam were supposed to be trapped in the proximal littoral to neritic areas (Jiang et al., 2015; Cui et al., 2018; Wang et al., 2019). By the Late Miocene, the paleo-geomorphology is known as a semi-closed horn--shaped depression that opened to the east with the terrain being high in the west and low in the east, along the Central Depression of the Qiongdongnan basin (Su et al., 2009, 2014; Cao et al., 2015; Shang et al., 2015; Chen et al., 2020).

The Central Canyon in the Qiongdongnan Basin has developed since the Late Miocene and acted as one of the major pathways for transporting sediments basinwards across the SCS margin (Su et al., 2009, 2014; Yuan, 2009; Liu et al., 2012; Cao et al., 2015). This canyon system was suggested as the main cross-slope supply route to the NWSB for sediments sourced from the paleo-Red River System and/or Central Vietnam-Hainan Island during the Late Miocene, feeding the potential submarine fan systems within the NWSB (Wang et al., 2011; Chen et al., 2015; Li et al., 2017). The fall of relative sea level and the structural inversion in the northern Yinggehai Basin during the Late Miocene might together facilitate such long-distance sediment transport (Cao et al., 2015). The structural high west of Hainan Island in Yinggehai Basin might affect sediment dispersal routes from the paleo-Red River system during the Late Miocene (Clift and Sun, 2006; Cao et al., 2015). However, this sediment pathway is no longer active, which might be due to tectonic subsidence of the Yinggehai Basin. In addition to the two principal pathways, the NW slope is cut by a number of smaller downslope canyons/channels, which also contribute sediment to the basin floor (Chen et al., 2013) (Figs. 1b and 2).

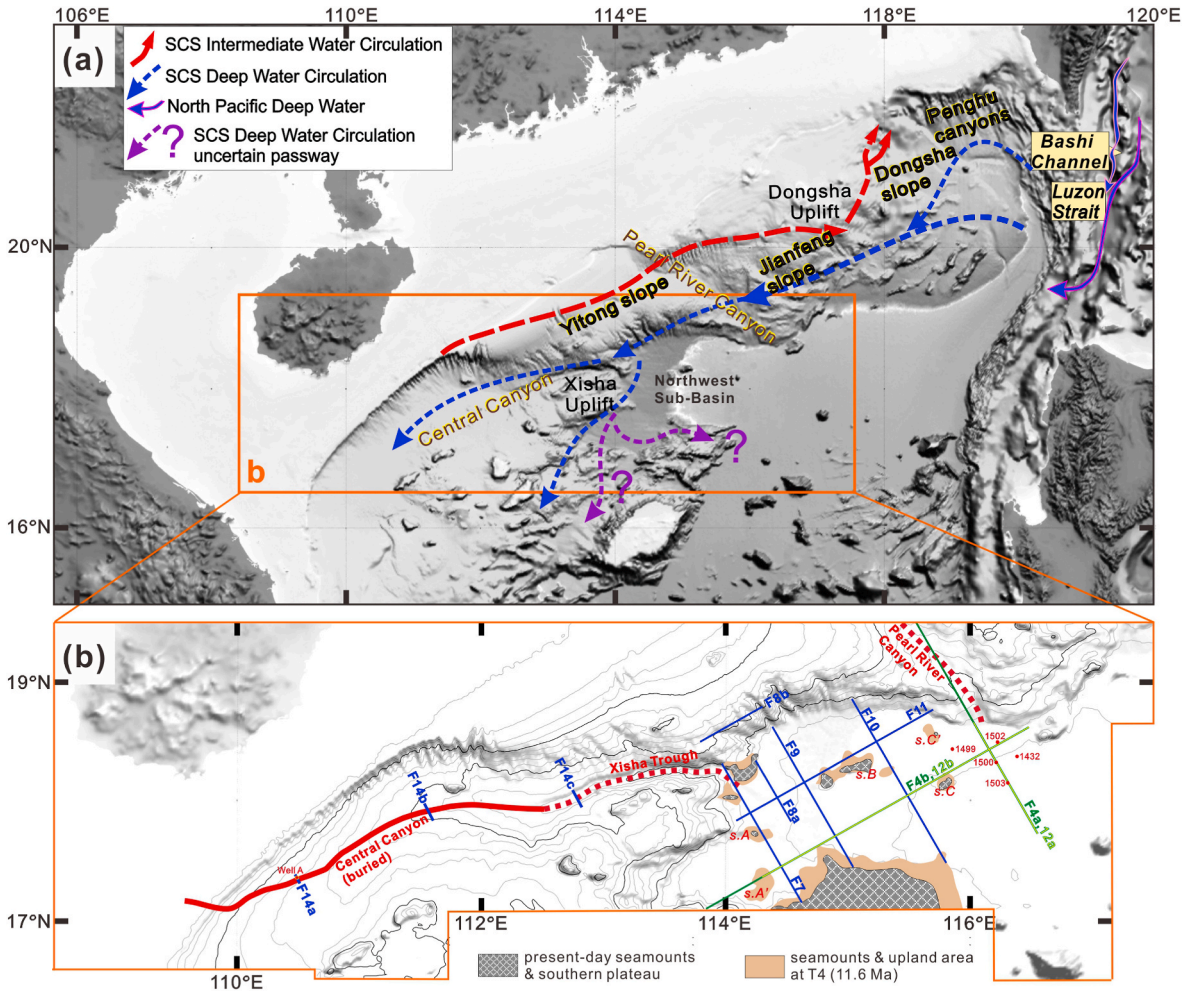

Fig. 2. A. Bathymetric map of the mid-northern part of the South China Sea (SCS) (published by Guangzhou Marine Geological Survey) showing the pathways for the intrusion of the Northwest Pacific Deep Water into SCS via the Bashi Channel/the Luzon Strait (the blue solid arrows, modified from Lüdmann et al., 2005); The assumed SCS Deep Water Circulation pathways in the mid-northern SCS (the blue dashed arrows; modified from Shao et al., 2007; Wang, 2007) and the assumed SCS Intermediate Water Circulation pathways in the mid-northern SCS (the red dashed arrows, modified from Zhu et al., 2010; Li et al., 2013; Wang et al., 2013) are indicated; The orange box is an inset of Fig. 2B; **B.** Bathymetric map of the Northwest Sub-Basin and surrounding area (extrapolated from 2D seismic data) showing locations of the studied 2D seismic profiles of Figs. 6–13, the industrial Well A (Huang et al., 2015; Shang et al., 2015) and IODP sites U1432, U1499, U1500, U1502 and 1503 (Larsen et al., 2018; Yin et al., 2018; Wu et al., 2018); The *s.A*/*s.A*′, *s.B*, and *s.C*/*s.C*′ represent the locations of the three seamounts involved in this study; The dotted red lines indicate the present-day Xisha Trough and Pearl River Canyon; The red line indicates the buried Central Canyon; Through tracking the reflection interface of 11.6 Ma (T4) and 0 Ma (present-day seafloor) over the study area, the seamounts and upland area at T4 and present-day are indicated by pink and grey areas, respectively. (For interpretation of the references to colour in this figure legend, the reader is referred to the Web version of this article.)

2.2. Oceanographic framework

The present-day oceanographic setting is one of a relatively large and deep marginal sea in which the modern circulation is driven by exchange with the Pacific Ocean through the Luzon Strait between the Philippines and Taiwan, and strongly influenced by its physiographic characteristics. Three principal water masses have been identified: surface water (0 m–~350 m), intermediate water (~350 m–~1350 m), and deep water (>~1350 m), although some authors make a further subdivision into deep and bottom water around 2000 m water depth (Gan et al., 2006; Wang and Li, 2009b; Yin et al., 2019) (Fig. 2b). The water exchange in the Luzon Strait plays an important role in the meridional turnover and horizontal circulation structure. It also leads to an active system of meso-scale eddies (100 km–160 km in diameter) and large internal waves propagating along the ~350 m interface (Zhao et al., 2014).

The bottom currents associated with the intermediate and deep circulation were established no later than the late Miocene (Chen et al., 2014), and gradually evolved into the modern SCS deep water mode during the middle Pleistocene transition (~1 Ma) (Lüdmann et al., 2005; Li et al., 2009; Wang and Li, 2009b; Zhao et al., 2009). The seafloor of the study area is currently swept by a cyclonic SCS Deep Water Circulation pattern, which has an overall flow velocity <5 cm/s, and mainly occurs below 1000 m (Xie et al., 2013; Wang et al., 2013, 2016; Shu et al., 2014; Zhao et al., 2015) (Fig. 2a). The invasion of the Northern Pacific Deep Water via the Luzon Straits is the predominant driving force for the cyclonic SCS Deep Water Circulation (Lan et al., 2013) (Fig. 2a).

3. Material and methods

A collection of over 5000 km multichannel 2D airgun reflection seismic profiles covering the NWSB area (about 35000 km^2) provided by the China National Offshore Oil Corporation was analysed. All seismic profiles are oriented either NNW-SSE (about 20 km spacing) or ENE–WSW (about 15 km spacing). Using an average P-wave velocity of 1500 m/s for the water column, the vertical scale of these profiles was converted from two-way travel time to depth for quantifying seabed morphologies.

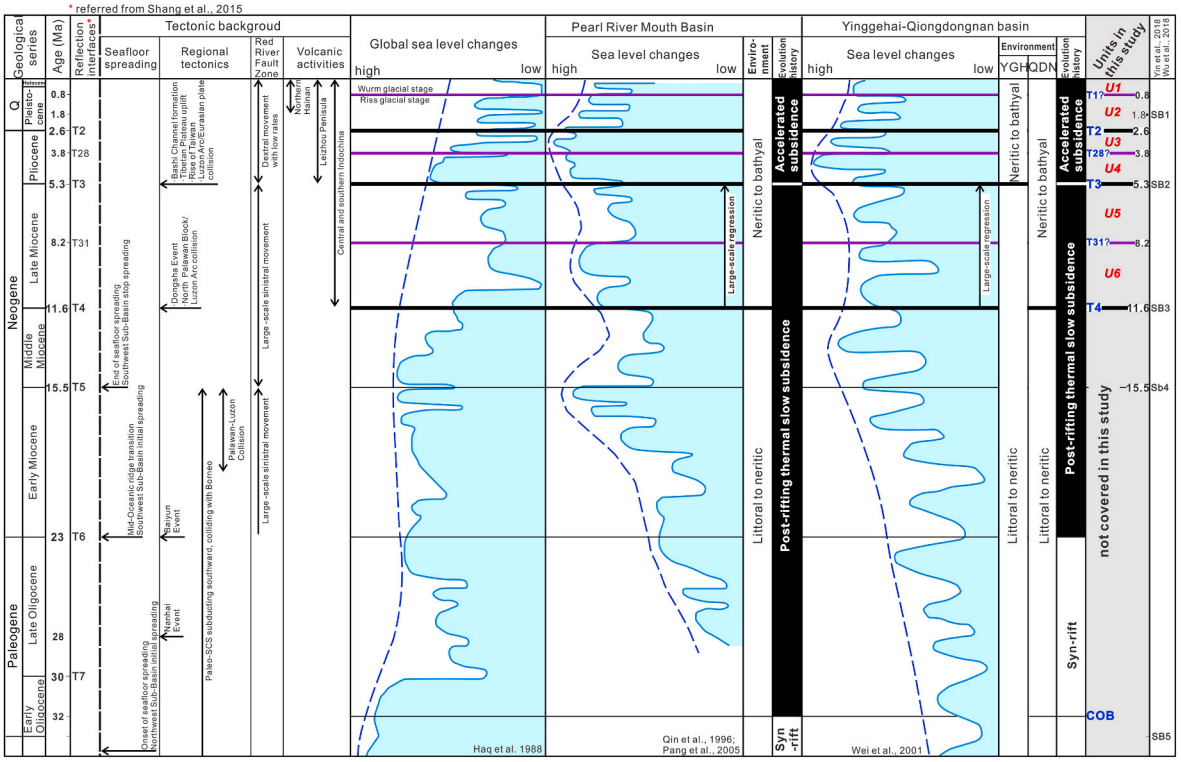

Fig. 3. Schematic overview of the major structural and tectonic/climatic events in the northern South China Sea since the Late Miocene (modified from Li et al., 2009; Yu et al., 2014) and their respective regional sea-level changes (Qin, 1996; Wei et al., 2001; Pang et al., 2005) with comparison to the global range (Haq et al., 1987); Seismic interfaces used in this study include T1 (1.8 Ma, assumed), T2 (2.6 Ma), T28 (3.8 Ma, assumed), T3 (5.3 Ma), T31 (8.2 Ma, assumed), T4 (11.6 Ma) and the crust ocean boundary (COB, 32 Ma) (Xie et al., 2008; Wu et al., 2018; Yin et al., 2018); Corresponding seismic units from U1 to U6 are indicated as well; Interpretation of the correlation seismic profile connecting IODP sites U1432, U1435, U1499, U1500 and U1502 were applied to derive the age constraint of strata from the Late Miocene onwards in the study area (Jian et al., 2018; Larsen et al., 2018; Wu et al., 2018; Yin et al., 2018).

The seismic signal was generated using a Bolt Longlife Airgun (3850 in^3 of volume), by means of compressed air (2000 psi). The record length and sampling rate were set at 11996 ms TWT and 2 ms, respectively. The acquired signals were recorded within 396 channels using a fold of 99, and lie in the frequency range of 40–60 Hz, allowing a vertical resolution up to 40 m. The data were processed through Omega V1.8.1 software, applying a bandpass filter (ranging from 6 Hz of low-cut frequency and 12 dB/s of low-cut slope to 136 Hz of high-cut frequency and 276 dB/s of high-cut slope), a de-noising and amplitude compensation and a post-stack time Kirchhoff migration. The processed seismic data were loaded into a Geoframe Suite (V4.5, 64-bit) project for horizon picking and sediment dynamics interpretations.

4. Results-seismic stratigraphy and seismic facies

Analysis of the seismic data is presented in two parts: (a) establishing the seismic stratigraphic framework since the Late Miocene (Figs. 3 and 4), and (b) documenting of the principal seismic facies (Fig. 5). In the following section, we consider the spatial distribution of architectural elements (Fig. 6).

4.1. Seismic stratigraphy

Four major regional stratigraphic surfaces since the late Miocene are identified, based on the reflector prominence and regional extent, as well as on minor reflector terminations against major reflectors. From base to top, these reflectors are identified as T4 to T1. They can be dated through correlation to the seismic profiles in the eastern part of this study area that intersect with IODP sites U1432, U1435, U1499, U1500 and U1502, resulting in reflector dates of T4 (11.6 Ma), T3 (5.3 Ma), T2 (2.6 Ma) and T1 (0.8 Ma, approximately) (Jian et al., 2018; Larsen et al., 2018; Wu et al., 2018; Yin et al., 2018) (Fig. 2b). Whereas reflectors T1 to T4 match those popularly identified in previous studies, we also recognize two further regional horizons that are less extensive and distinct, but nevertheless prominent reflectors against which local reflector terminations occur. These are designated and speculated as T28 (3.8 Ma) between T2 and T3, and T31 (8.2 Ma) between T3 and T4 (e.g., Shang et al., 2015) (Figs. 3 and 4).

These six named reflectors divide the late Miocene to recent succession into six seismic units, U1 to U6. Seismic units U1 and U2 are Quaternary, U3 and U4 are Pliocene, and U5 and U6 are late Miocene in age. Together, the U1-U6 succession in the past 11.6 Ma accounts for over 65% of the basin fill, whereas the portion from T4 to basement (the crust ocean boundary, COB, Yin et al., 2018), at an estimated age of 32 Ma, represents much slower rates of sedimentation.

4.1.1. Late Miocene seismic units (U5 and U6)

The Late Miocene succession lies between the high-amplitude basal reflector T4 (11.6 Ma) and reflector T3 (5.3 Ma), and is sub-divided here into two seismic units, U5 and U6, separated by reflector T31 (8.2 Ma). Both units can be distinguished from the overlying and underlying succession, due to their overall prominently higher amplitude reflections (Figs. 4 and 7–11). They mainly consist of continuous to discontinuous, parallel and sub-parallel, high amplitude reflectors. Locally, the reflectors are of lower amplitude, and in places there are patches of chaotic, low-amplitude to transparent reflections (see yellow packages in Figs. 8a, 9–12). Within the lower U6 seismic unit, moderate to high amplitude reflectors display onlap/downlap relationship onto the seismic reflector T4 (Figs. 4b, 7 and 10, 11). Compared to U6, seismic unit U5 shows more high amplitude reflection packages, and is 1.5 times as thick (Figs. 4 and 7–12). In the central part of the NWSB, the thickness of U5 and U6 combined can reach more than 700 ms TWT (e.

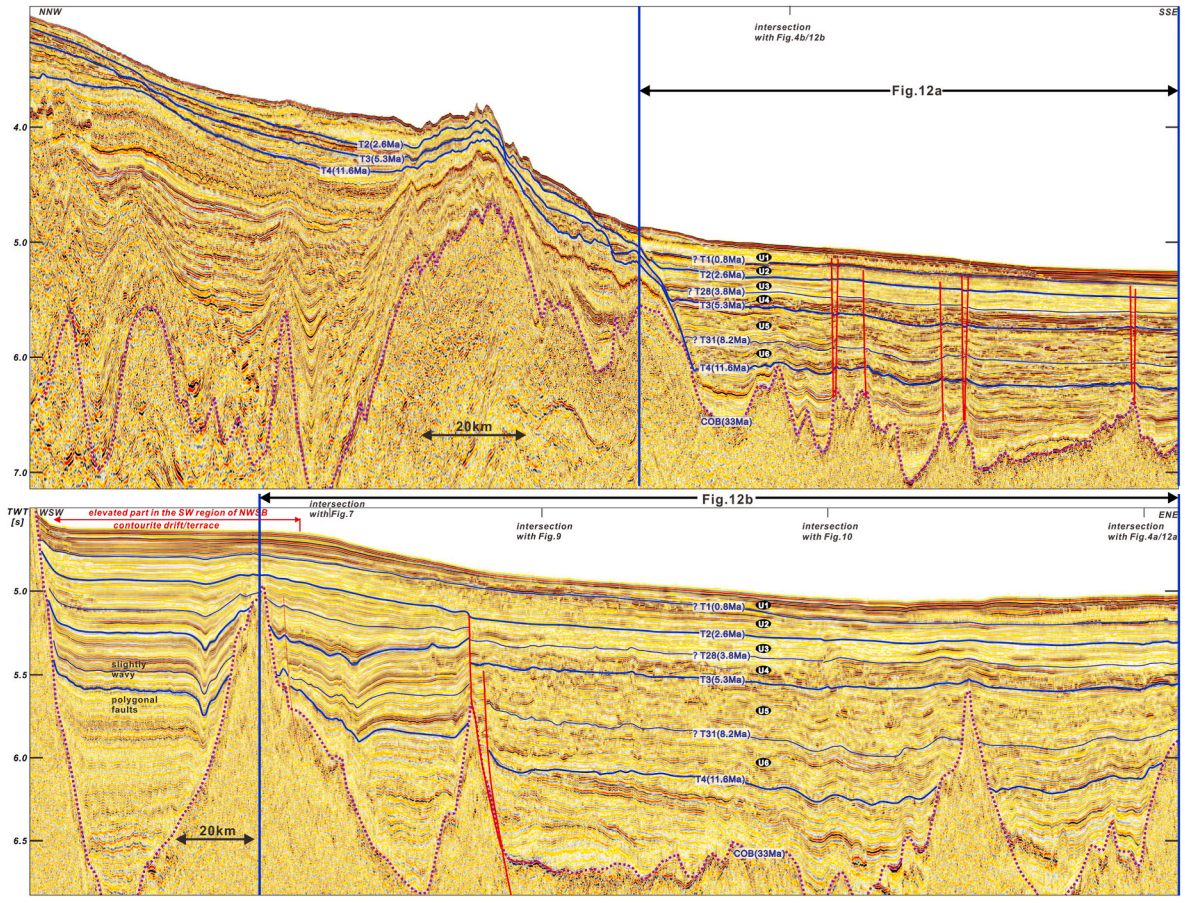

Fig. 4. Seismic stratigraphic framework in the northern South China Sea in this study; see locations of the seismic profiles in Fig. 2B.

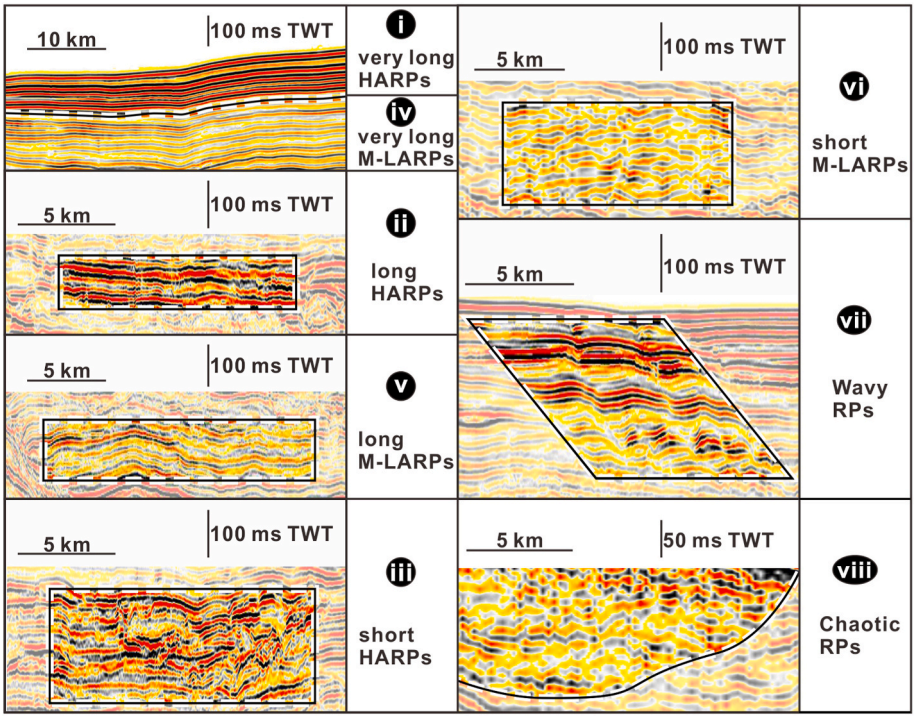

Fig. 5. Overview of the eight groups of encountered seismic facies in this study; (**I**) = Very long high amplitude reflection packages (HARPs); (**II**) = Long HARPs; (**III**) = Short HARPs; (**IV**) = Very long moderate-low amplitude reflection packages (M-LARPs); (**V**) = Long M-LARPs; (**VI**) = Short M-LARPs; (**VII**) = Wavy RPs; (**VIII**) = Chaotic RPs.

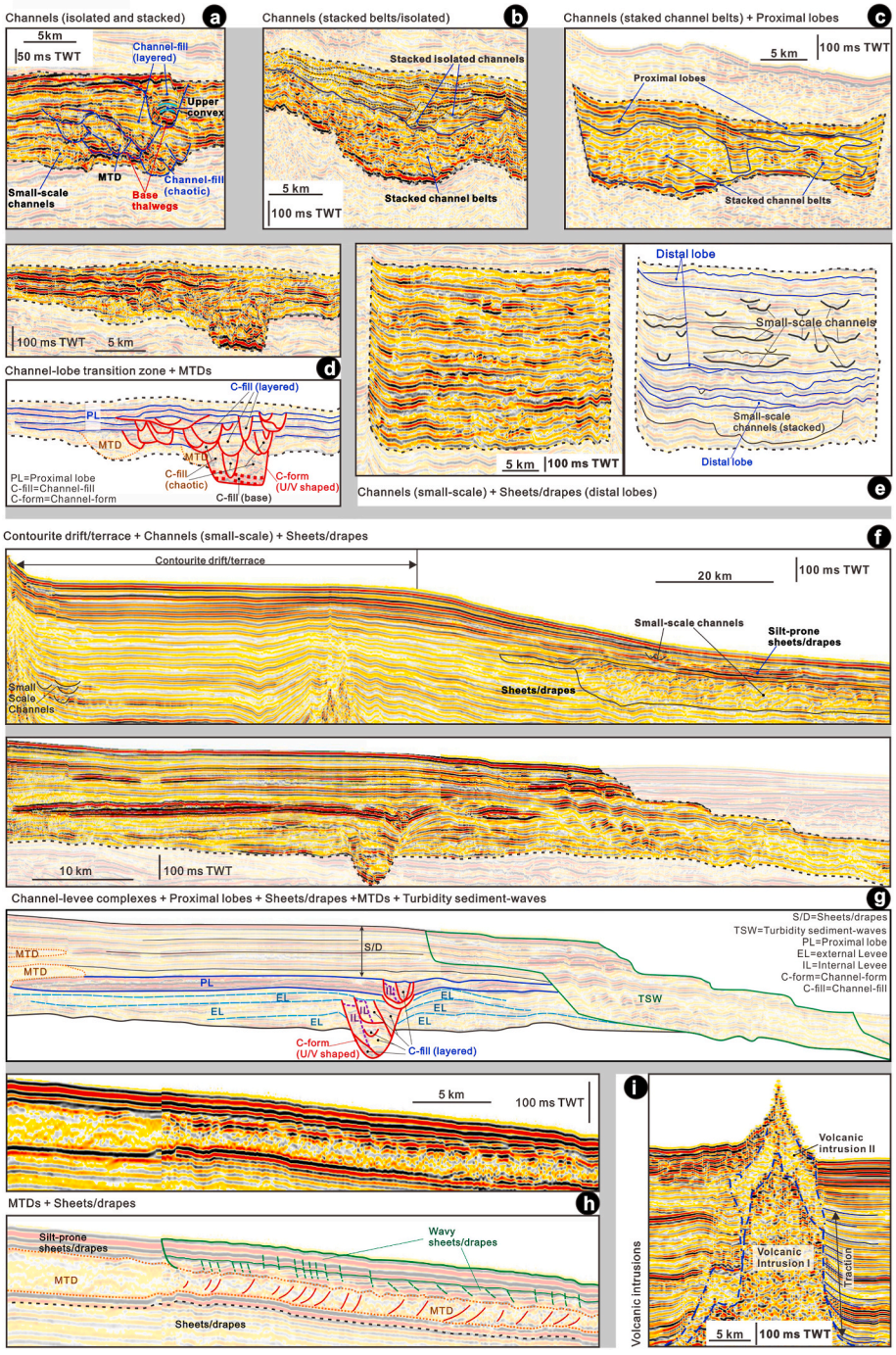

Fig. 6. Overview of the seven groups of possible architectural elements interpreted from seismic faces in this study; (**A**) = Isolated and stacked channels; (**B**) = Stacked channels belts/isolated channels (**C**) = Stacked channel belts and proximal lobes; (**D**) = Channel-lobe transition zone and mass-transport deposits (MTDs); (**E**) = Small scale channels and sheets/drapes; (**F**) = Contourite drift/terrace, small scale channels and sheets/drapes; (**G**) = Channel-levee complexes, proximal lobes, sheets/drapes, MTDs and proposed turbidity sediment-waves; (**H**) = MTDs and sheets/drapes; (**I**) = Volcanic intrusions .

g., Figs. 8a and 9–11). This decreases in the SW of the basin to less than 400 ms TWT (Figs. 4b, 11 and 12b).

4.1.2. *Pliocene seismic units (U3 and U4)*

The Pliocene succession lies between seismic reflector T3 (5.3 Ma) and T2 (2.6 Ma). It is subdivided here into seismic units U3 and U4 by reflector T28 (3.8 Ma). Compared to the late Miocene (U5 and U6), seismic units U3 and U4 contain a larger proportion of moderate to low amplitude reflection packages and mostly continuous and semi-continuous reflectors (Figs. 4 and 9–11). U4 has less than half the proportion of itself with high amplitude reflection packages (both continuous and chaotic). U3 contains even less high amplitude reflection packages compared to U4 (high-amplitude packages are indicated in orange with black line shading in Figs. 8a and 9–12), and has many more continuous reflection packages and contains some layered chaotic and wavy intervals. The average thickness of the Pliocene succession (U3 and U4) in the major central part of the NWSB ranges from 250 ms to 300 ms TWT, which is about half that of the Late Miocene interval (Figs. 4 and 7–12). This increases over the SW region of NWSB to around 400 ms TWT, similar to that of the Late Miocene interval (Figs. 4, 7 and 11).

4.1.3. *Quaternary seismic units (U1 and U2)*

The Quaternary succession is bounded at its base by T2 (2.6 Ma) and topped by the present-day seafloor (0 Ma). It is subdivided into seismic units U1 and U2, separated by reflector T1 (0.8 Ma). U1 and U2 generally contain the most continuous and parallel reflections throughout the sedimentary sequence, with varying amplitudes from

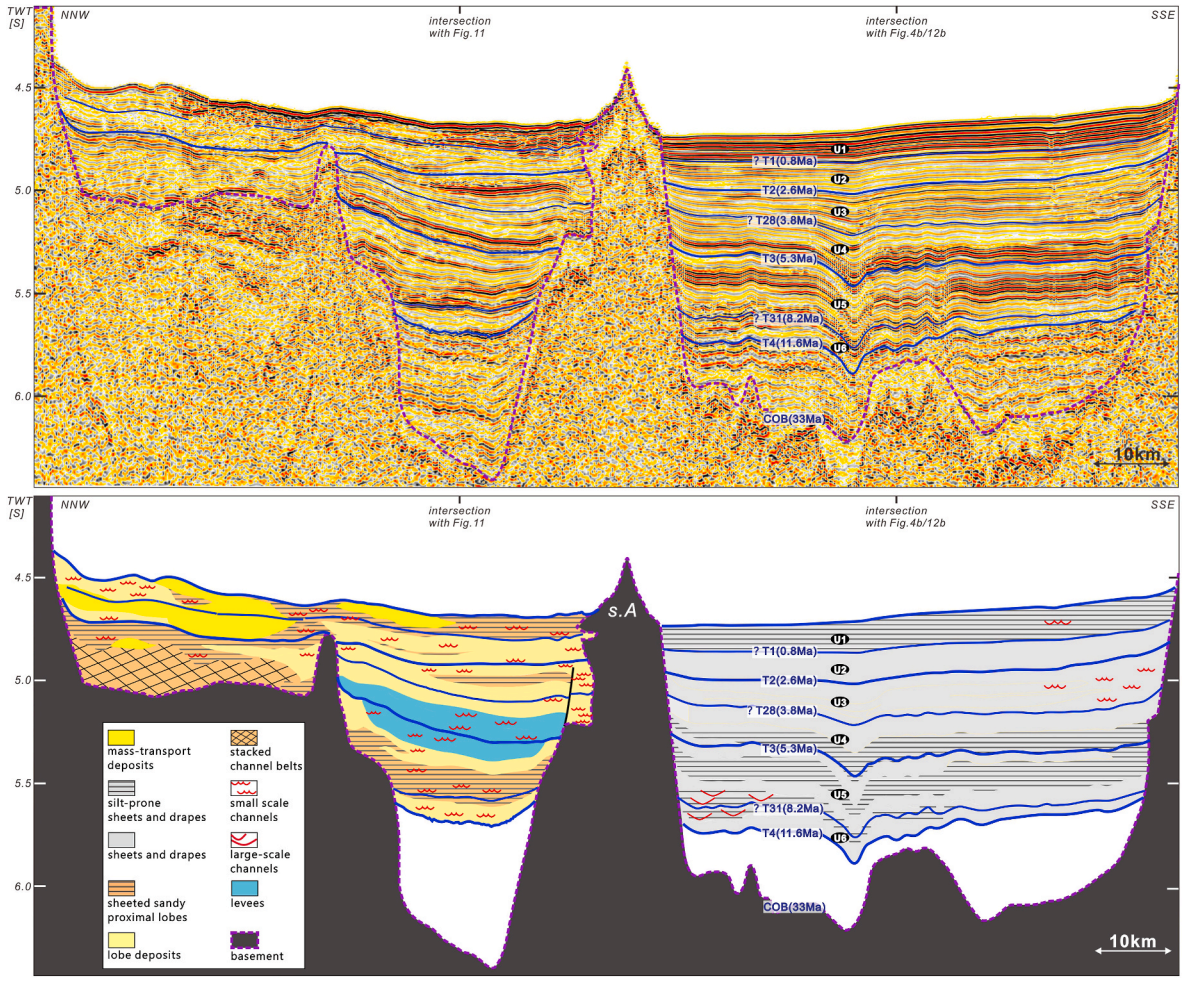

Fig. 7. NNW-SSE oriented seismic profile (see its location in Fig. 2B) with seismic interfaces (Above) and architectural element interpretations (Below).

moderate to high (Figs. 3, 4 and 7–11). Chaotic, wavy low amplitude to transparent reflections occasionally disrupt the reflection continuity (see yellow and green packages respectively within Figs. 7, 8a and 9, 10 and 12). U1 has generally higher amplitude reflections than U2 (Figs. 4, 7, 8, 10 and 11). The average thickness of the Quaternary (U1 and U2) in the major central part of the NWSB ranges from 150 ms to 200 ms TWT, and increases to about 300 ms TWT in the SW of the basin (Figs. 4, 7 and 11).

4.2. Seismic facies

Eight different seismic facies are distinguished on the basis of the external geometry (such as reflector amplitude, orientation, continuity) and internal architecture (such as reflector contact relationship, uniform or chaotic). These can be grouped as: (1) High-Amplitude Reflection Packages (HARPS), (2) Moderate to Low-Amplitude Reflection Packages (M-LARPS), and (3) Non-uniform Reflection Packages. Within the first two, a further sub-division can be made according to reflector continuity, using a somewhat arbitrary reflector length. Hence, *very long* refers to continuous reflectors >20 km, *long* refers to reflectors of 5 km–20 km, and *short* refers to reflectors <5 km. The non-uniform reflectors may be *wavy* or *chaotic*.

4.2.1. High-Amplitude Reflection Packages (HARPs)

4.2.1.1. Seismic facies I and II: very long and long HARPs. These seismic facies are characterized by continuous to semi-continuous, parallel to sub-parallel, moderate to high amplitude reflectors (Fig. 5i and 5ii). They are sub-divided into two distinct seismic facies on the basis of reflector continuity. Very long HARPS (seismic facies I, Fig. 5i) are designated as those with continuous reflectors over 20 km in length, but in fact many of these are continuous over 50 km and more. Long HARPS (seismic facies II, Fig. 5ii) are where the reflector continuity is restricted to less than 20 km, but typically ranging between 5 km and 15 km.

Seismic facies I is relatively uncommon and is mainly restricted in occurrence to U1, and more rarely in U3 and U4 (Figs. 4 and 7–12). Over the SW corner and edge regions of the NWSB, very long HARPS occur in layers within U1, U4 to U6 (Figs. 4b and 7). Seismic facies II is more common in the central parts of the basin, especially in parts of U4, U5 and U6 (Figs. 4 and 9–12).

4.2.1.2. Seismic facies III: short HARPs. Short HARPs occur as isolated intervals of short (<5 km) high-amplitude seismic reflectors, which are typically discontinuous and sub-parallel in superimposed complexes (seismic facies III, Fig. 5iii). In many cases, they co-occur with more chaotic reflector packets in U- to V-shaped channel incision forms, at various scales, which can incise markedly into the underlying succession. Seismic facies III is most concentrated within the central part of the study area, and especially common during the deposition of units U5 and U6, becoming much less common from U4 upwards (Figs. 8a and 9–11).

4.2.2. Moderate to Low-Amplitude Reflection Packages (M-LARPs)

4.2.2.1. Seismic facies IV and V: very long and long M-LARPs. These seismic facies feature continuous to semi-continuous, parallel to sub-

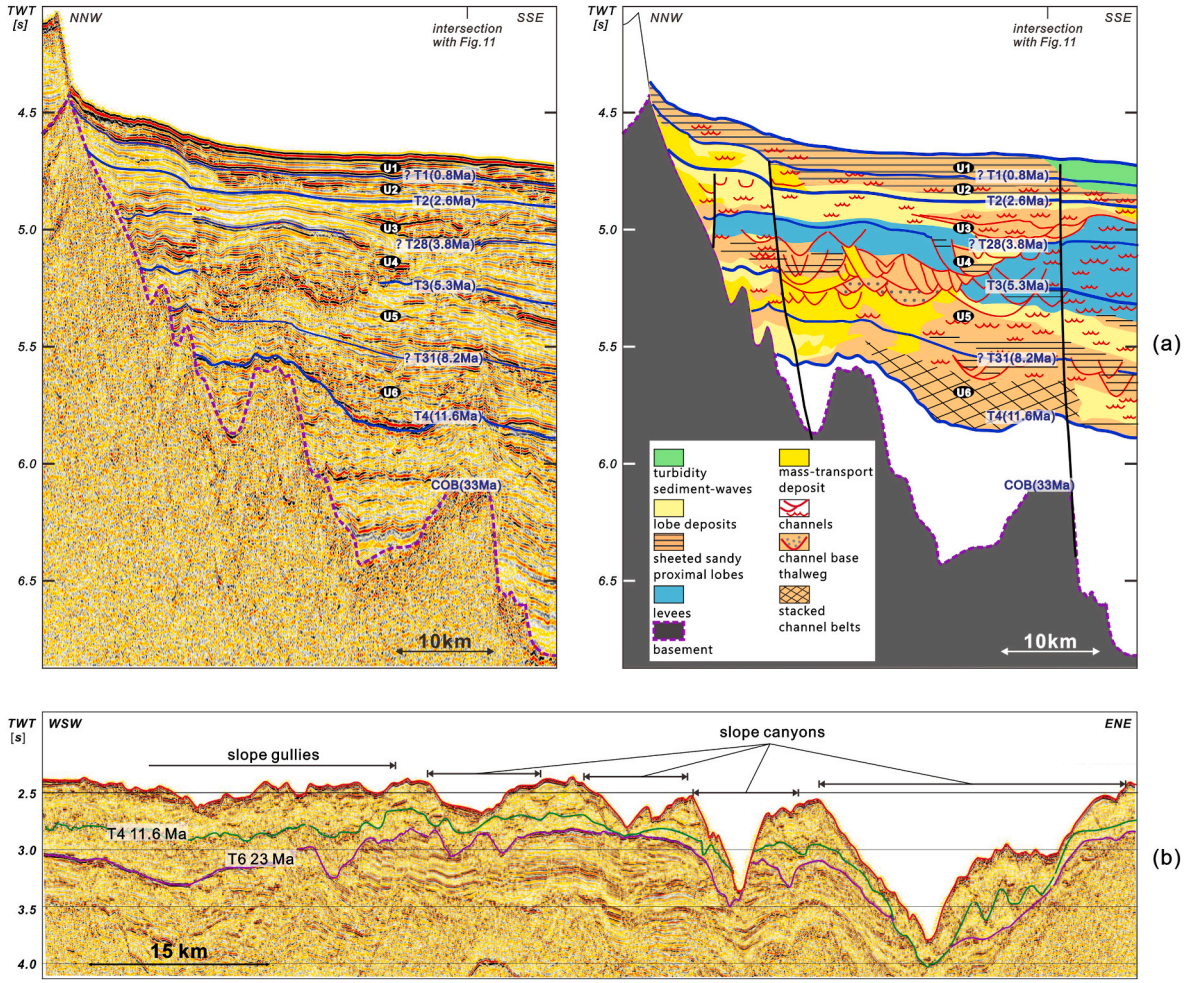

Fig. 8. A. NNW-SSE oriented seismic profile (see its location in Fig. 2B) with seismic interfaces (Left) and architectural element interpretations (Right); **B.** WSW-ENE oriented seismic profile (see its location in Fig. 2B) showing with seismic interfaces and architectural element interpretations.

parallel, moderate to low amplitude reflections (Fig. 5iv, v). They are sub-divided into two distinct types on the basis of reflector continuity. Very long M-LARPS (seismic facies IV, Fig. 5iv) show laterally extensive reflectors (over 20 km) with very small gradients of amplitude, which have an overall sheet-like form. Long M-LARPs (seismic facies V, Fig. 5v) are less extensive (limited within 20 km and the majority ranging between 5 km and 10 km), slightly convergent towards topographic highs or basin edges, and broaden into basin depressions.

Seismic facies IV is concentrated within seismic units U2 and U3, and partly shown in U1 and the upper part of U4 (Figs. 4 and 9–12). It is discovered appearing vertically through U2 to U6, especially covering the SW corner of the NWSB (Figs. 4b and 7). Seismic facies V is more recognised within U4 to U6, focusing the appearance in the central NWSB and usually in adjacent with long and short HARPs (Figs. 4 and 7–12).

4.2.2.2. Seismic facies VI: short M-LARPs. Short M-LARPs are closely comparable with short HARPS. They occur as isolated intervals of short (<5 km) moderate to low-amplitude seismic reflectors, which are typically discontinuous and sub-parallel within vertically-stacked (or superimposed) complexes (Fig. 5vi). In many cases, they co-occur with short HARPS and more chaotic reflector packages in U- to V-shaped channel incisions. These incisions can excavate the underlying succession up to 200 ms TWT. Seismic facies VI occur throughout the succession (U1 to U6), and especially in the more western margin of the basin (i.e., close to the exit of the Xisha Trough, Figs. 7 8 and 11).

4.2.3. Non-uniform reflection packages

Two further seismic facies are commonly observed through the NWSB succession that are different from the generally horizontal reflection packages (above), but also quite distinct from each other. Both are common in deep-water settings everywhere over the world.

4.2.3.1. Seismic facies VII: wavy reflection packages (WRPs). The WRP seismic facies refers to packages of continuous to semi-continuous, low to moderate-amplitude reflectors (more rarely high-amplitude), with a symmetrical to asymmetrical wave-shaped geometry (Fig. 5vii). The reflectors within the package are parallel to sub-parallel and may extend over 10 km–40 km of seismic line. These WRPs are most evident in parts of seismic units U1, U2 and U3 (Figs. 8a and 9–12), but in lower units the irregular wavy shapes might also be occasionally observed (e.g., see U5 and U6 in Fig. 4b and U4 in Fig. 11). One conspicuous example occurs vertically throughout U1 to U3 with a thickness of over 400 ms TWT in Fig. 9. The wave-like form appears to be, in part, inherited from the T28 boundary (3.8 Ma) at the top of U4. The wave forms typically have an average wavelength of ~2 km and wave height of ~30 ms TWT (Figs., 5vii, 8, 9 and 11). The orientation of the wave crests and the area over which they occur cannot be determined from our limited 2D seismic data. The other conspicuous example of WRPs in the study area have average wavelengths of within ~1 km, wave heights less than 10 ms TWT and extension of less than 20 km, which is restricted in occurrence to seismic units U1 and U2 (e.g., Figs. 10 and 12a, b). In most cases, WRPs pass laterally and vertically into long or very long parallel reflectors of the M-LARP seismic facies.

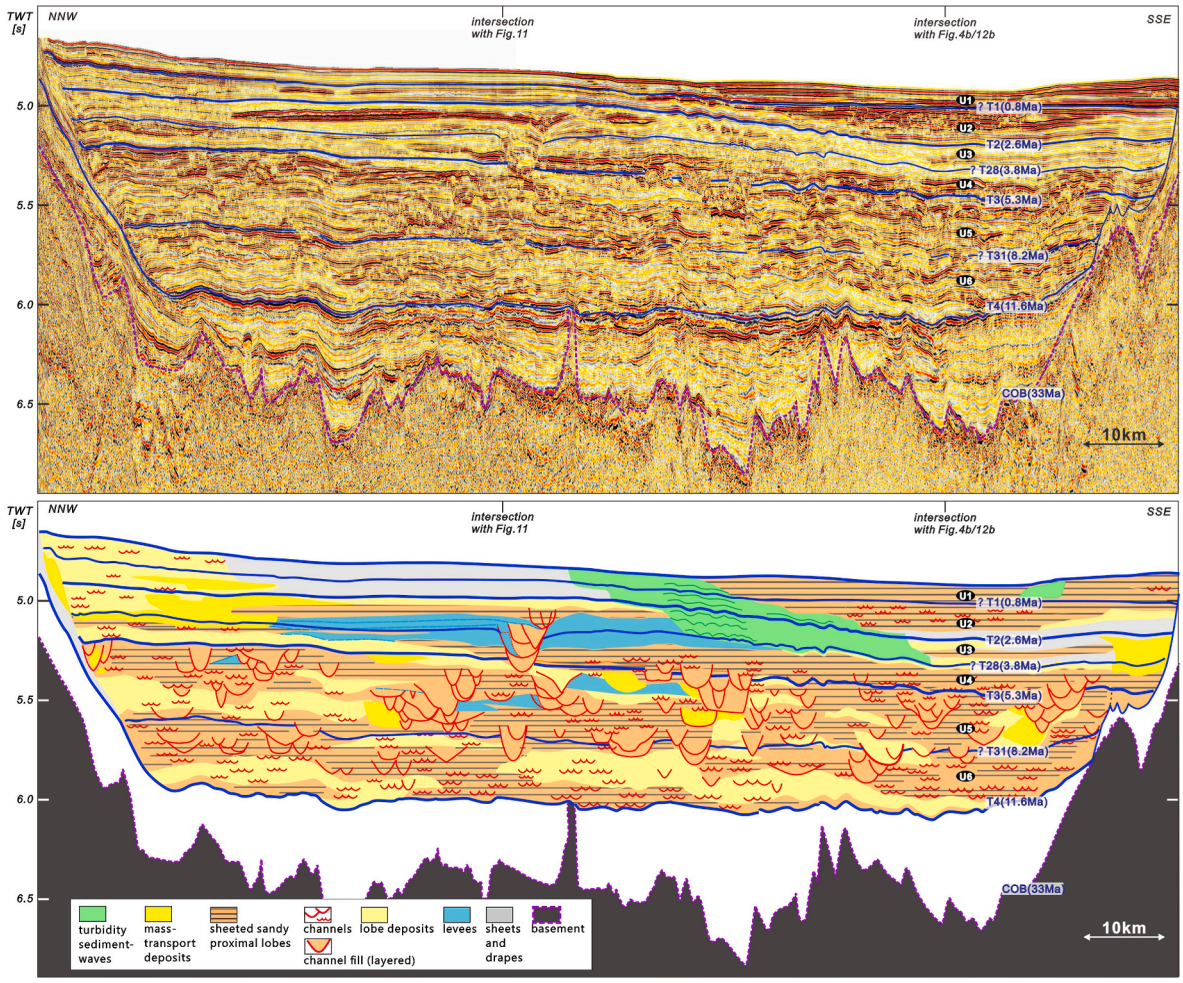

Fig. 9. NNW-SSE oriented seismic profile (see its location in Fig. 2B) with seismic interfaces (Above) and architectural element interpretations (Below).

4.2.3.2. Seismic facies VIII: chaotic reflection packages (CRPs). The CRP seismic facies are distinguished by an absence of any distinct reflectors. Even when very short reflectors are present, there is a chaotic matrix of reflector spots, almost as a hazy blur of indistinct seismic reflection (Fig. 5viii). In the study area, there are two types: those that are distinctly rooted on the acoustic basement (e.g., Fig. 7) and those that occur entirely within the sedimentary succession (e.g., Fig. 12a). The former are mostly present as inverted conical forms or narrow spikes intruding into the sediment. The latter occur either as irregular elongate forms (>10 km long) interbedded within the normal succession of other seismic facies, or as the partial fill of erosive, channel-like features (e.g., Fig. 9), where they are commonly associated with short HARP and short M-LARP seismic facies (typically ≪ 10 km). They are recognised throughout the NWSB succession, especially close to the basin margin slopes and within large channels (Figs. 7–9 and 11 and 12).

5. Seismic interpretation of architectural elements

Architectural elements within the NWSB can be interpreted on the basis of their seismic facies (above), their geometry and the occurrence or distribution of the recognised features. Channels, levees, lobes, sheets and drapes, MTDs, volcanic intrusions and some other elements with a less clear interpretation have been identified (Fig. 6, Table S1).

5.1. Channels

Isolated channels, stacked channels and channel complexes of different scales are recognised. They are interpreted from the channel-shaped incisions, and irregular fill of CRPs, short HARPs and short M-LARPs.

5.1.1. Large isolated and stacked channels

These show clear U and V-shaped outlines cutting into underlying reflectors, with incision widths from 5 to 8 km and depths from 100 ms to 200 ms TWT (Figs. 6a, b and 13a). In some cases, several separate, vertically stacked incisions can be observed indicating a long-lasting conduit that remained in more or less the same location through time (<1–3 Ma). Channel fill typically comprises a mixture of short parallel high amplitude reflectors (Fig. 6a and b), short parallel moderate to low amplitude reflectors (Fig. 6b and c), chaotic low amplitude to transparent reflection packages and contorted to chaotic high amplitude reflection packages (Fig. 6d). The short parallel reflectors most likely represent turbidites, with or without interbedded hemipelagites, for which the high-amplitude reflectors indicate a higher proportion of coarse-grained turbidites (Kastens and Shor, 1986; Piper et al., 1999; Deptuck et al., 2008). Inclined, high amplitude curved and chaotic reflector patterns indicate the rather irregular nature of channel fill processes, with separate channel thalwegs, lateral accretion packages, localized MTD input, and some slip planes, faults, and slumped structures caused by differential compaction between muddy and sandy intervals (Posamentier, 2003; Mayall et al., 2006; Janocko et al., 2013). The chaotic low-amplitude to transparent reflection packages most likely represent MTDs (see interpretation below in section ***5.5***). Packages of discontinuous chaotic high amplitude reflections occurring at the channel bases could be coarser-grained material (e.g., thick-bedded turbidites and amalgamated lag deposits) carried in the lower parts of

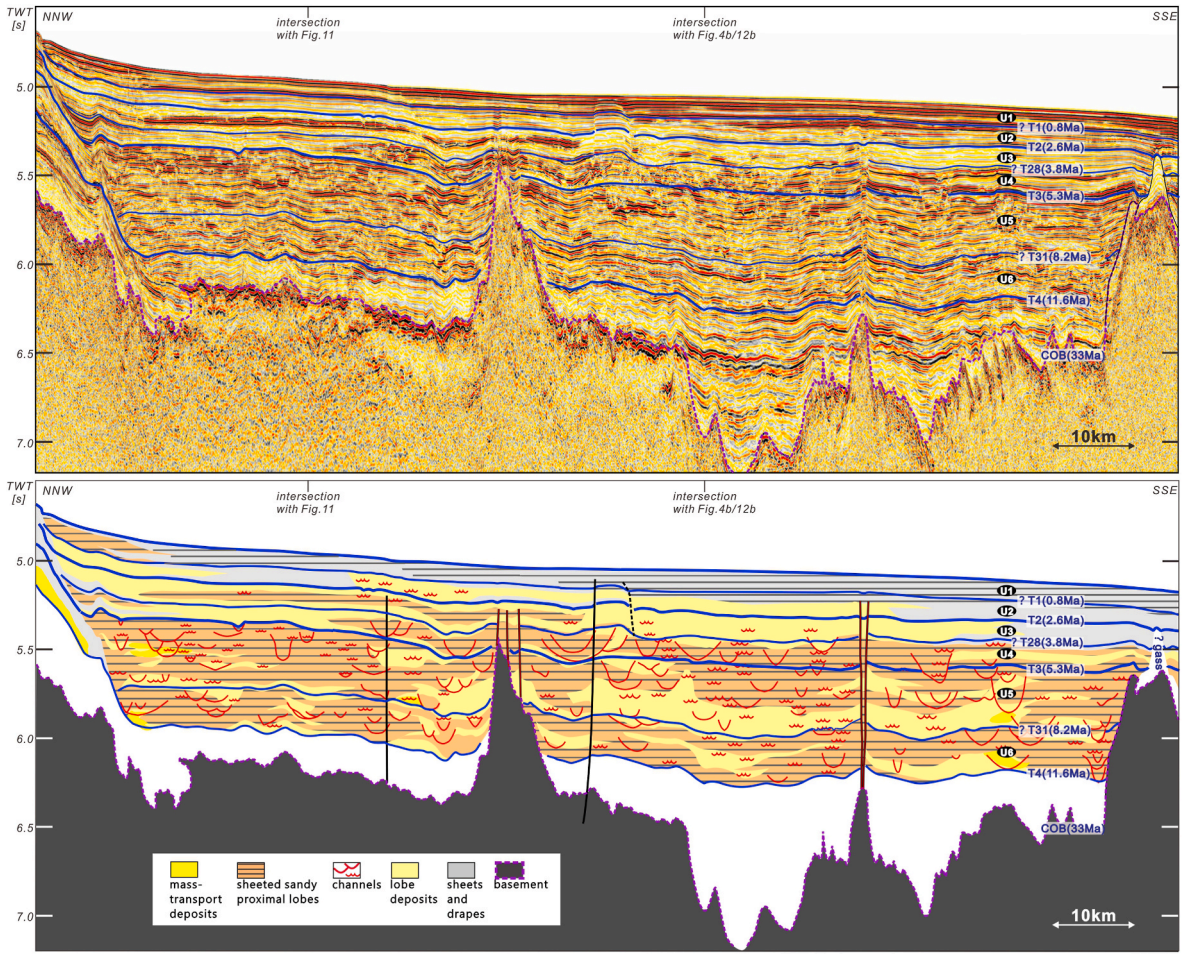

Fig. 10. NNW-SSE oriented seismic profile (see its location in Fig. 2B) with seismic interfaces (Above) and architectural element interpretations (Below).

turbidity currents (Kneller and McCaffrey, 1995; Hiscott et al., 1997; Lopez, 2001; Schwenk et al., 2005).

5.1.2. Channel complexes

An association of smaller channel-like features that are clustered at the basinward exit of the Xisha Trough show small to indistinct incisions, and an irregular distribution of short HARPs and short M-LARPs within a more regular background seismic facies. These could be interpreted as stacked channel belts fed from the Xisha Trough (Figs. 6b and c, 7, 8, 11 and 13a), similar to those stacked channels which are straight or sinuous with high sandy fill content (Watson, 1981; Mayall and Stewart, 2000; Mayall et al., 2006). Channel widths, where these can be inferred from seismic data, range from 2 km to 5 km.

In a more basinward location, intervals of mixed irregular reflections of both short HARPs and short M-LARPs (Figs. 6d, e, 6f and 13c), are interpreted as small-scale channels, erosional scours or small-scale coarse-grained bedforms. These may represent the channel-lobe transition zone on a submarine fans, which is typically a zone of irregular erosion, deposition and sand-rich facies (basinward of a feeder channel) that can also be recorded in the seismic facies (e.g., Wynn et al., 2002; Brooks et al., 2018). Similar facies are reported off the northern margin of East Corsica and on the Hueneme and Dume submarine fans offshore California (Piper et al., 1999; Deptuck et al., 2008). Mixed irregular reflection intervals with high amplitude (e.g., Fig. 6d) may correspond to coarser sediments from more proximal fan regions (the upper middle fan), while intervals with moderate amplitudes could be coarser sediments within the middle-lower fan.

The channel complexes with distinctively high amplitude reflectors share many characteristics with the architectural elements in the upper fan channel-belts on the Niger Delta slope, the Amazon Fan, the Cenozoic Congo Fan, and the Middle Bengal Fan (Lopez, 2001; Deptuck et al., 2003; Schwenk et al., 2005; Kolla et al., 2007; Bastia et al., 2010).

Accordingly, the large isolated/stacked channels and stacked channel belts interpreted in this study are assigned as a part of the root/upper fan part, while the channel-lobe transition zone is taken as a part of the middle-lower fan part (Fig. 13a, c).

5.2. Channel-levee complexes

The combination of channel erosive forms and channel fill seismic facies together with long M-LARPs forming a wedge-shape depositional geometry away from one or both channel margins, is interpreted as representing channel-levee complexes (Fig. 6g). These wedge-shaped packets show continuous, low-to moderate-amplitude reflectors, typically with slight convergence and dimming away from the channel flank, and can be considered as external levees (e.g., Hansen et al., 2015) (see EL in Fig. 6g). Internal downlap surfaces are commonly present and, more rarely, toplap surfaces as a result of truncation by overlying strata. Packets of continuous to discontinuous, moderate-to high-amplitude reflectors with irregular wedge-shaped geometry within larger channel forms are interpreted as internal levees (Kane and Hodgson 2011; Hansen et al., 2015) (see IL in Fig. 6g). These are bench-like depositional terraces within channels, adjacent to the channel margin and external levees, which have been widely recognised within the upper-middle parts of submarine fans (Pirmez and Flood, 1995; Lopez, 2001; Deptuck et al., 2003; Schwenk et al., 2005). The channel-levee complexes

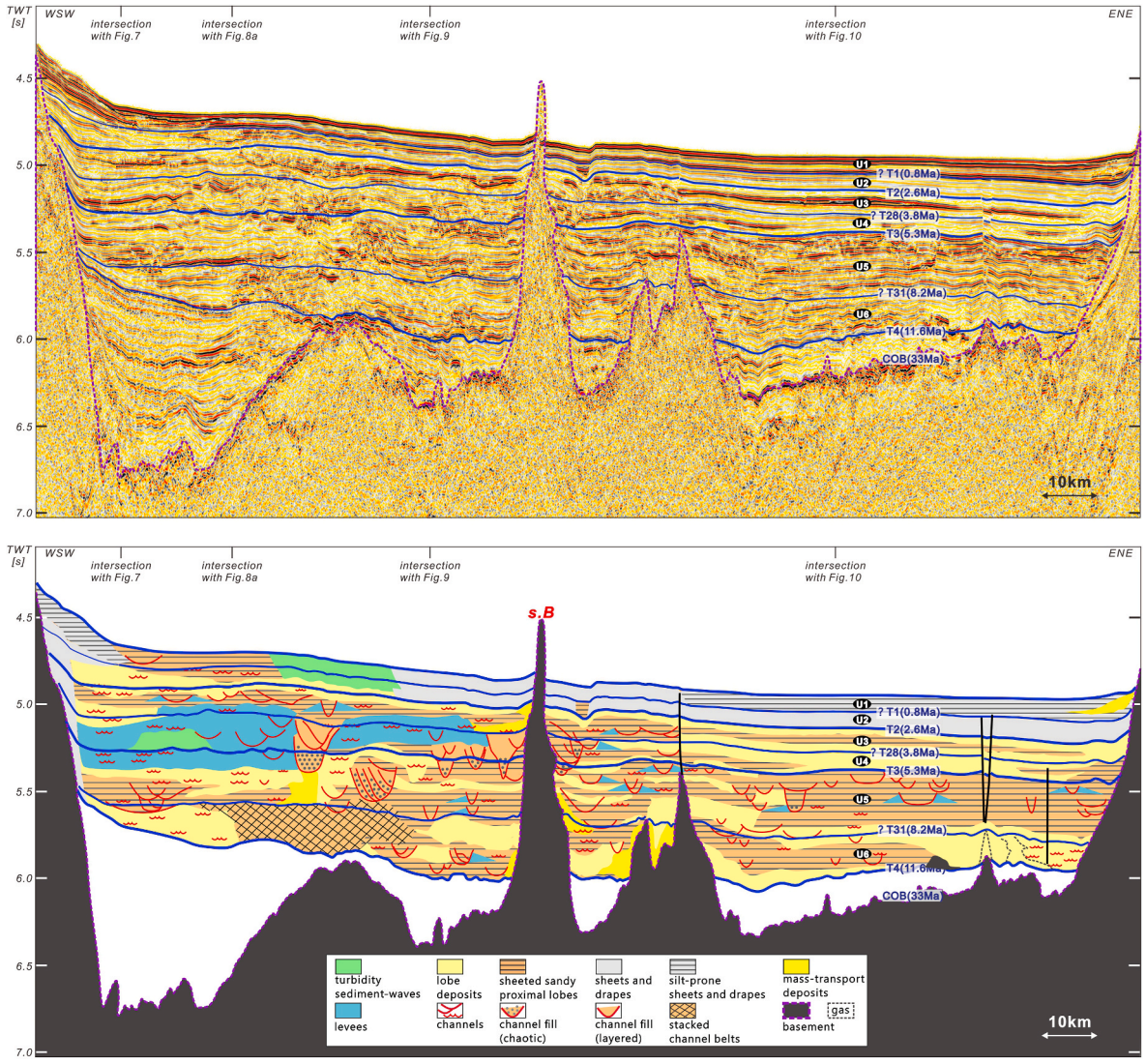

Fig. 11. WSW-ENE oriented seismic profile (see its location in Fig. 2B) with seismic interfaces (Above) and architectural element interpretations (Below).

recognised in this study are assigned to an upper-middle fan part (Fig. 13b).

5.3. Lobe deposits

Lobes are extremely difficult to interpret based on 2D seismic profiles alone. They have very subtle, broad lenticular geometries, which show almost no expression in the subsurface when deeply buried. However, proximal lobes are generally more sand-rich, which may be recorded by high-amplitude reflectors, and also by multiple small incisions from distributary channels (as the very terminal parts where small channel may be active concurrently) (e.g., Vittori et al., 2000). Through a combination of these features and their location within the basin, some of the long and very long HARPs are interpreted as proximal lobes, especially where they are associated with minor channels and irregularities (Fig. 6d and g).

The terminology of HARPs was first applied for reflector packages corresponding to thick beds of fine- or medium-grained massive to graded sands within the Amazon Fan (Flood and Piper, 1997). On the upper and middle Amazon Fan, these packages are the result of channel avulsions/levee breaches followed by un-channelized turbidity currents flowing in intra-channel lows. On the lower fan, they represent sandy lobes at the termination of channel-levee systems (Lopez, 2001; Pirmez and Flood, 1995; Schwenk et al., 2005). Similar seismic facies have been interpreted as sand or silt-prone turbidites interbedded with mud-rich sediments on composite mid-fan lobes and proximal isolated lobes in other fan systems (Piper et al., 1999; Deptuck et al., 2008).

Accordingly, long and very long HARPs associated with channel belts or channel-levee complexes in the present study are interpreted as sheeted sandy proximal lobes on the NWSB upper-middle fan systems (Fig. 13b and c). These pass down-fan into more distal lobes (Fig. 13d), with thin-bedded, fine-grained turbidites and interbedded hemipelagites, represented by long M-LARP seismic facies, in some cases with associated short M-LARPs (Fig. 6e).

5.4. Sheets and drapes

Long and very long M-LARP seismic facies commonly show a sheet-like geometry and occur as sediment fill to the central parts of the basin (Fig. 6f–i). They are typically thicker in the basin centre and show slight convergence towards topographic highs and the basin margin or, in some cases, more distinct seismic onlap (Figs. 4b, 7 and 11). These sheeted architectural elements, we interpret as mainly thin-bedded, fine-grained basin-floor turbidites, interbedded with hemipelagites (e.g., Stow, 1985b; Bouma, 2000). In common with similar seismic facies described from other deep-water systems, they are interpreted to be

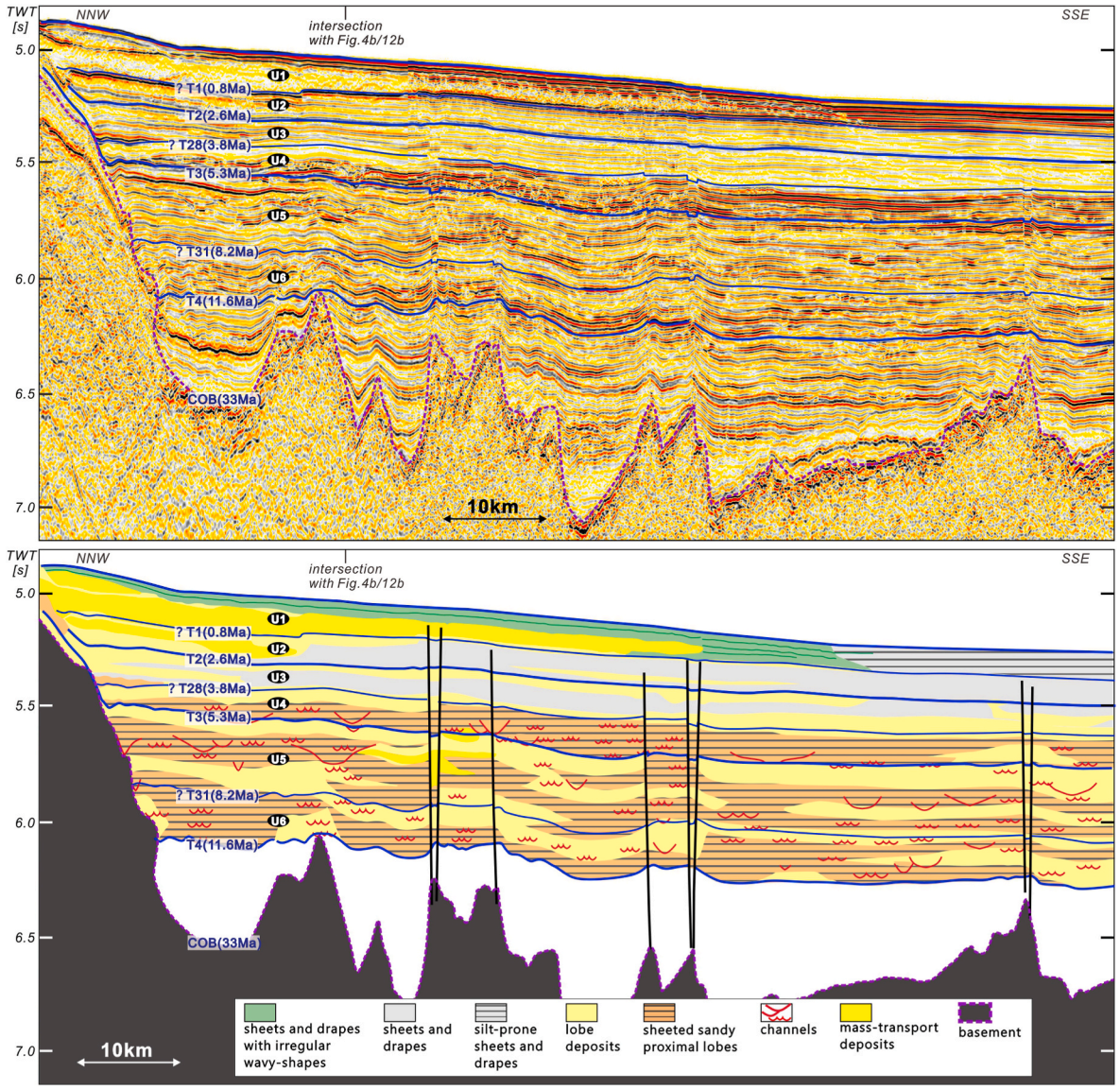

Fig. 12. **A**. NNW-SSE oriented profile (see its location in Fig. 2B) with seismic interfaces (Above) and architectural element interpretations (Below); **B.** WSW-ENE oriented profile (see its location in Fig. 2B) with seismic interfaces (Above) and architectural element interpretations (Below).

mainly mud-rich with a few silt and sand beds (Piper et al., 1999; Deptuck et al., 2008). Very long HARPs with similar sheeted geometry and occurrence are widespread over the basin fill within U1 (Figs. 7–12), and such high amplitude reflections (Figs. 5i and 6f–i) may again be interpreted as silt-prone thin-bedded, fine-grained turbidites inter-bedded with mud-rich hemipelagites (Piper et al., 1999; Deptuck et al., 2008).

On slopes surrounding the basin, we observe similar seismic facies with sheet-like geometry in places, or with a more drape-like geometry (e.g., Figs. 10–12). This draped architectural element is less evident in the basin centre but is not easy to distinguish from the sheeted geometry. Where the drape form is dominant, it is interpreted as a more hemipelagite-rich assemblage.

5.5. MTDs and volcanic intrusions

MTDs are most readily recognised in seismic profiles as irregular mounded forms with low amplitude to transparent CRPs (Fig. 6h). They occur inter-layered within the normal fan/basin succession, especially close to the basin slopes, or as the partial fill of large erosive channels (Fig. 13a). These are interpreted as mass wasting deposits derived either from surrounding slopes and/or from channel margin collapse.

CRPs that are rooted in the basement are interpreted as volcanic highs, seamounts, and intrusions, which in this study mainly derive from the former spreading ridges (Yin et al., 2018). They typically exhibit cone-shaped highs of various size and many of them are buried beneath the T4 reflector (Figs. 8a, 9 and 12a), whereas others are large enough to have intruded into the overlying Late Miocene to Recent sedimentary succession and some to pierce through the seafloor and have a prominent topographic expression (Figs. 1, 7, 10 and 112b). High amplitude reflectors are present where these rooted CRPs are in contact with the surrounding sedimentary layers. Seismic reflectors are seen to onlap onto the rooted CRPs and pinch-out against the steeper slopes of the cone-shaped highs (Figs. 6i, 7 and 10, 11, 12b).

5.6. Other architectural elements

5.6.1. Wavy reflector packages (WRPs)

The principle WRP that extends through U1-U3 and over 20 km laterally (Figs. 9 and 11), is comparable in scale and wave dimensions

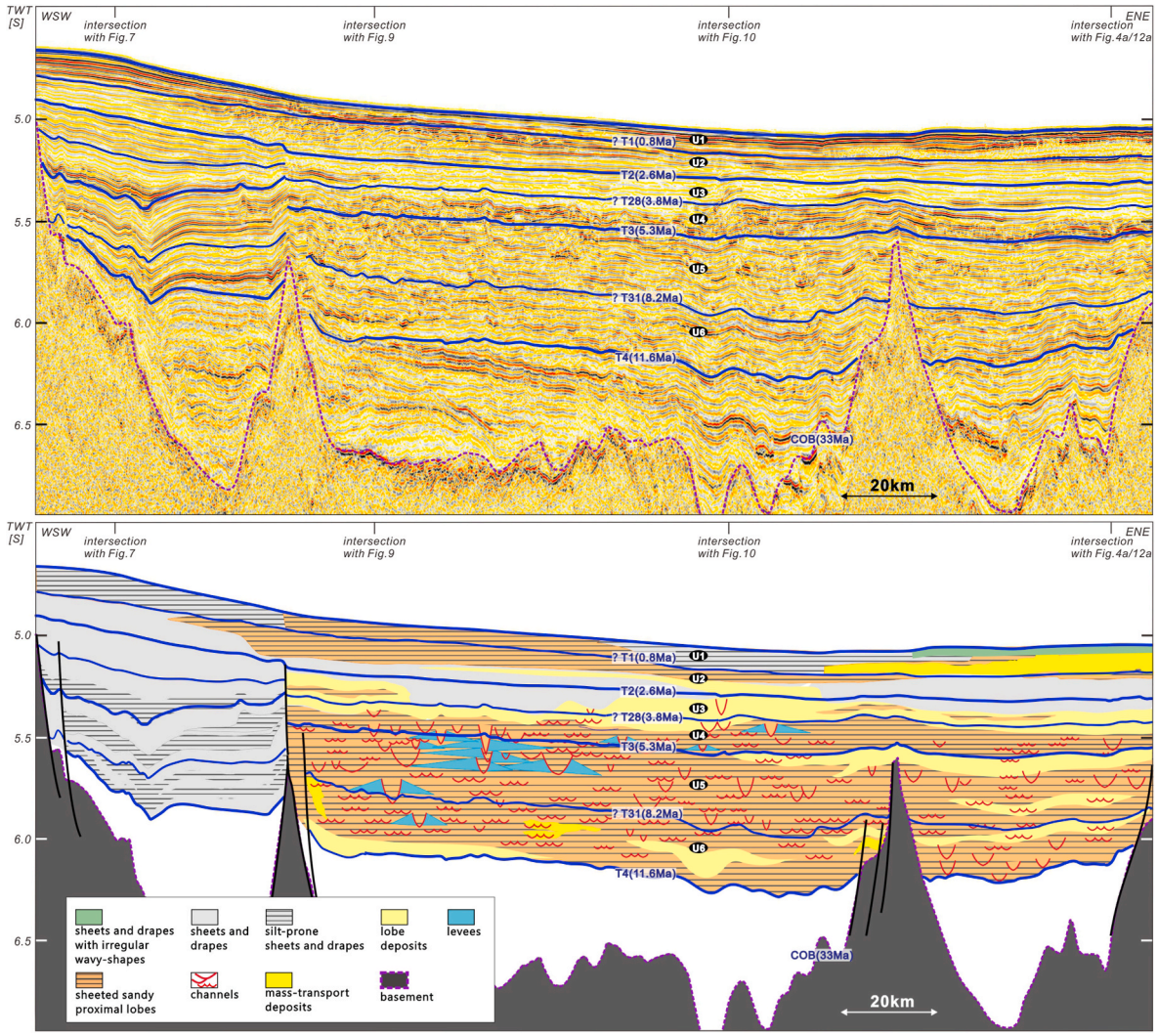

Fig. 12. (*continued*).

with both bottom current and turbidity current wave systems (Wynn and Stow, 2002). Considering the proximity to channels, we propose these wavy sediments to be dominated by turbidity current overspill processes (Cartigny et al., 2011, Fig. 13b). Rather irregular wavy shapes also occur within U1 (Fig. 12a and b), but their irregularity and extent seem to be more closely linked to the overlying MTDs than to any current-driven wave-forming process (Fig. 6h). Reflectors within U5 and U6 over the SW edge of the NWSB are slightly wavy. This appears to be directly related with an underlying polygonal fault system (Fig. 4b).

5.6.2. *Contourite drift/terrace*

In contrast to the central part of NWSB, its southwest corner is covered with thick succession of both very long and long HARPs and M-LARPs throughout U1 to U6 (Figs. 4b and 6f). This region is built up above the level of the basin plain but has no clear turbidity current input. Considering the uniformity and regularity of the seismic reflectors, as well as its slightly elevated (~150 m) seabed topography (comparable with a contourite terrace), these sediments are attributed a contouritic origin (i.e., as sheeted drifts) (Faugères et al., 1999; de Haas et al., 2003), or at least strongly reworked by bottom currents (i.e., a contourite terrace). For further confirmation, however, additional sedimentary/observational/numerical simulating results are required, which is beyond the scope of this study but will be investigated in future endeavours.

6. Discussion

6.1. *Basin-floor submarine fan systems in the NWSB*

The NWSB is topographically a basin plain setting with two large supply systems: the Xisha Trough and Central Canyon from the west (Figs. 2b, 14 and 15), and the Pearl River Canyon from the northeast (Figs. 1 and 15). These are known to have had a long history and most likely acted as the two major feeder systems of prolonged sediment supply into the basin (Ding et al., 2013; Li et al., 2017; Sun et al., 2018a, b; Liang et al., 2019). The spatial and temporal evolution of basin-floor fans (Figs. 15i–iii and 16) proposed in this study are based on seismic facies and corresponding interpreted sedimentary facies of basin-floor fan systems since the Late Miocene. Seismic lines reveal that the basin fill sequences since the Late Miocene (11.6–0 Ma) can reach more than 1.2 s TWT, corresponding to a decompacted sediment thickness of more than 1000 m on average (locally as much as 1500 m). Its overall average sedimentation rate reaches ~10 cm/ky, which is almost three times as much as the rate from the Late Oligocene to Middle Miocene (~3.5 cm/ky). The total sedimentary budget for the Late Miocene was approximately 2680 km^3/My, for the Pliocene it was approximately 1280 km^3/My, and for the Quaternary it was approximately 2250 km^3/My (estimated by Wu et al. (2018) using the program Flex-Decomp™ by Kusznir et al. (1995) after time-depth conversion, Fig. 15iv–vi).

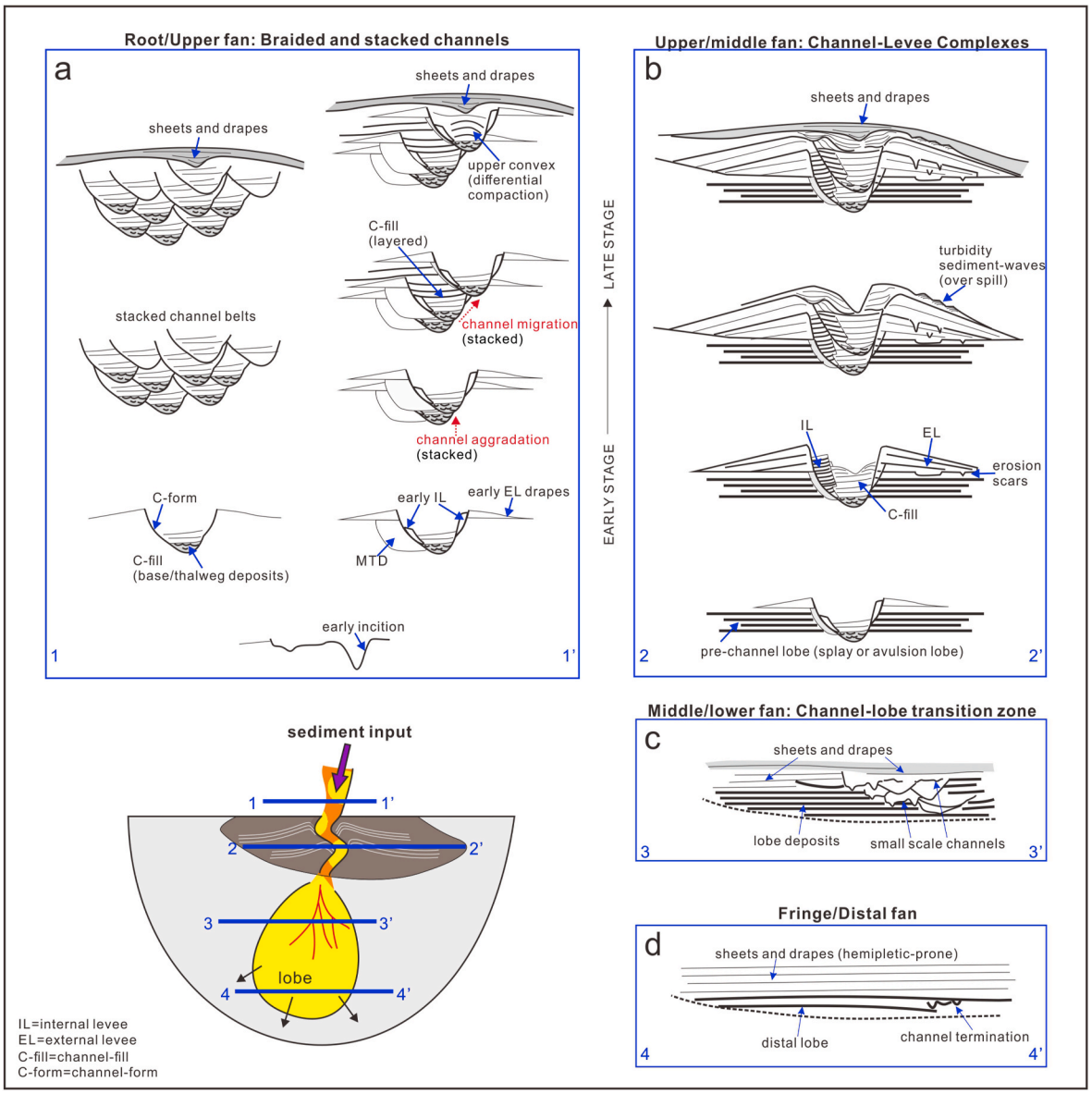

Fig. 13. Conceptional vertical development patterns of the submarine fan systems (the intersection in the lower left corner is modified from Normark, 1970; 1978); (a) 1-1' = Root-upper fan (stacked channel belts); (b) 2-2' = Upper-middle fan (channel-levee complexes); (c) 3-3' = Middle-lower fan (channel-lobe transition zone, small-scale channels, lobe deposits and sheets/drapes); 4-4' = Fringe/distal fan (small scale channel terminations, distal lobes and hemiplegic-prone sheets/drapes).

As outlined in the results section, a series of deep-water architectural elements has been identified; channels, levees, lobes, sheets and drapes, MTDs, turbidity sediment-wave fields and a contourite drift or terrace. These build a thick basin-fill succession since the Late Miocene. Apart from the contourite drift/terrace, which is confined to the SW corner of the basin, these elements and their spatial and temporal distribution, are most readily interpreted as parts of at least two large, basin-floor fan systems filling the NWSB since the Late Miocene (Fig. 13).

Due to a regional geographical relationship between the two fan systems and the Xisha Trough and the Pearl River Canyon as the most probable respective major feeder systems, the one occupying the western NWSB is named the Xisha basin-floor fan and the one occupying the eastern NWSB as the Pearl River basin-floor fan, respectively (Fig. 15i–iii). These are abbreviated to *Xisha fan* and *Pearl River fan*, respectively.

6.2. *Prospective evolution of the Central Canyon and Xisha fan*

In the context of the Xisha fan, it is important to consider evolution of the supply system through the Xisha Trough and Central Canyon to the west (Figs. 2b and 14), based on previous work (Xie et al., 2016; Cao et al., 2015; Li et al., 2017). The Central Canyon has a length of ~425 km and extends along the Central depression of the Qiongdongnan basin, which can be traced westward to the Yinggehai Basin and eastward into the Xisha Trough and NWSB (Su et al., 2009; Wang et al., 2012). At present, the western segment of the canyon has been filled (Fig. 14a and b), but the eastern segment of the Qiongdongnan basin (1500 m water depth) and in the Xisha Trough (Fig. 14c) remains only partially filled. Depositional evidence indicates that an open horn-shaped epicontinental sea developed along the Central depression of the Qiongdongnan basin since the Early Miocene (Xie et al., 2016). The Central Canyon was formed at the end of the Middle Miocene more or less along the thalweg of the epicontinental sea (Wang et al., 2015) (Fig. 16a).

Based on the analysis of high precision 2D and 3D seismic data, evolution and fill of the Central Canyon in the Qiongdongnan basin has the following characteristics (Shang et al., 2015; Xie et al., 2016) (Figs. 14–16). (1) Canyon erosion and transport stage (T4/11.6 Ma-T31/8.2 Ma): Canyon formation at the end of the Middle Miocene.

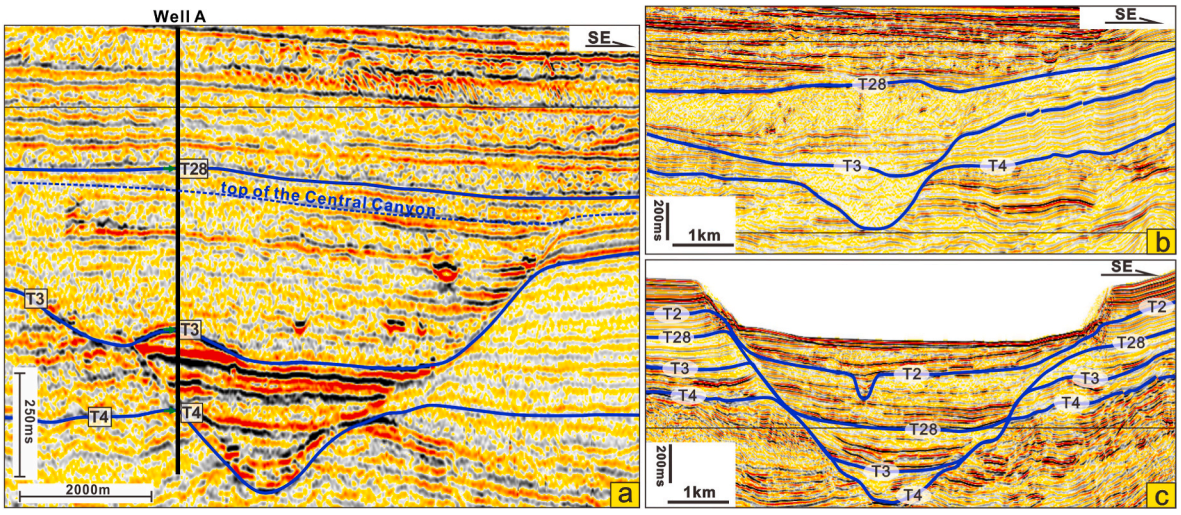

Fig. 14. A. Seismic-well tie and seismic facies interpretation within the Central Canyon fill (after Huang et al., 2015; Shang et al., 2015; Chen et al., 2020); **B and C.** The different fill-up time and sedimentary filling features within the Central Canyon from west to east; See Fig. 2B for the location of the Well A and the profiles.

Gravity flows carrying sediment from the west, including the Red River system, Central Vietnam and Hainan Island (Chen et al., 2014; Cao et al., 2015; Jiang et al., 2015; Cui et al., 2018), along the canyon thalweg during the early stage of the Late Miocene. Most of these early sediments were expected transporting eastwards and entering the NWSB, which led to the down-cutting morphology within the Central Canyon (Fig. 14). (2) Canyon fill stage (T31/8.2 Ma-T28/3.8 Ma): The onset of major canyon fill, with the interbedding of turbidites and MTDs (Fig. 14), possibly the former from the western source (Red River system, Central Vietnam) and the latter from the northern continental slope (mainly the Hainan Island) (Shang et al., 2015; Chen et al., 2020); decrease of turbidites and increase of MTDs upwards (Fig. 14), and an apparent decrease (/increase) relative proportion from the western (/Hainan) sediment supply possibly due to the paleo coastline locations (Jiang et al., 2015). (3) Canyon fill MTD stage (T28/3.8 Ma-T0/0 Ma): Due to the sudden weakening of sediment supply capacity from the western source, MTDs from the northern slope and southern uplift zone are taken as the main sediment supply to the canyon (Shang et al., 2015; Chen et al., 2020). Much of this material may remain in the canyon, such that the western segment is fully filled, but the eastern segment and the Xisha Trough remain open up to the Present (Fig. 14).

This evolution of the conduit system could be reflected in the inferred development of the Xisha fan (Figs. 15i–iii and 16). During the Late Miocene, a shelf edge delta at the westernmost domain of the Qiongdongnan Basin could feed the paleo Central Canyon with sufficient supply (Wang et al., 2011; Cao et al., 2015; Chen et al., 2015; Jiang et al., 2015; Cui et al., 2018) and throughput to enable formation of the Xisha fan (Figs. 15i and 16a). With a possible sharp decrease in sediment supply since the Pliocene (Shang et al., 2015; Chen et al., 2020) (Fig. 14), the scale of the Xisha fan should correspondingly decrease markedly (Figs. 7, 8a and 9, 11 and 15ii). This may be related to cessation of the delta-feed to the west of the canyon (Shang et al., 2015; Chen et al., 2020) (Fig. 16b), which might have been linked to dextral strike-slip tectonic activity within the Yinggehai Basin at around 5.3 Ma (Cao et al., 2015; Jiang et al., 2015; Shang et al., 2015). After T28/3.8 Ma, very little sediment was suggested transporting from the Central Canyon through the Xisha Trough to the NWSB (Su et al., 2009, 2011, 2014; He et al., 2011; Shang et al., 2015) (Figs. 14 and 16b). This could lead to a further shrinkage of the fan system since T28/3.8 Ma, and to the final evolution into a rather small abyssal fan system with no clear fan lobes during the Quaternary (Figs. 7, 8a and 9, 11, 15iii and 16b).

Although currently there is no more precise evidence to show the relationship between the Central Canyon/Xisha Trough and the Xisha fan, because of the lack of deep drilling in the western NWSB, it may be inferred that the Late Miocene-Early Pliocene (U4, U5 and U6) Xisha fan was majorly derived most likely from the west based on the channel architecture, element distribution and depositional thickness (Figs. 7, 8a and 9, 11 and 15i–15ii). If this is the case, changes in sediment supply should dominantly controlled the depositional infilling processes of the Central Canyon and in turn the size of the submarine fan system in the NWSB.

6.3. *Possible spatial and temporal evolution of basin-floor fans*

Two large deep-water channel systems are believed to have provided the principal sediment supply into the NWSB. The Central Canyon and Xisha Trough in the west can derive sediment from east Vietnam and the Red River System (Wang et al., 2015) (Fig. 16a). Although the general sedimentary environment in the Qiongdongnan Basin varied from shallow water to bathyal during the Late Miocene, the ancient Red River Delta west of the Central Canyon served as a continuous sediment source (Su et al., 2009; He et al., 2013; Chen et al., 2015). The Pearl River Canyon in the NE can derive sediment from south and central China via the Pearl River. Additional supply could be derived from slope collapse and mass-transport processes (Figs. 7, 8a and 9), and from a series of smaller slope canyons/channels crossing the northern margin (Figs. 1b, 8b and 15 and 16). The variation in sediment supply for the NSWB would correspond with the supply status of these various input systems.

The possible spatial and temporal evolution of the two main basin-floor fan systems throughout the six units of U5-U6 (Late Miocene), U3-U4 (Pliocene) and U1-U2 (Quaternary) are indicated in Figs. 15 and 16, together with the corresponding decompacted thicknesses of sediments from Wu et al. (2018).

6.3.1. *Late Miocene*

During the Late Miocene, the sedimentary budget of the NWSB reached a maximum (~2680 km^3/My, ~12 cm/ky of the sedimentation rate, Wu et al., 2018). In the western part of NWSB, there may have two separate depocentres at the northern and southern sides of the seamounts *s.B*, which can correspond with supply from the Xisha Trough to the Xisha fan, and separation into two principle fan lobes on either side of the seamount chain. In the eastern part of the basin, there can have a further depocentre, which may correspond with supply to the Pearl River fan, and which is also partly interrupted by the seamount *s.C*. It is inferred that during this period both conduits were active and much sediment supplied (Su, 2011; Mao, 2015; Chen et al., 2020), resulting in

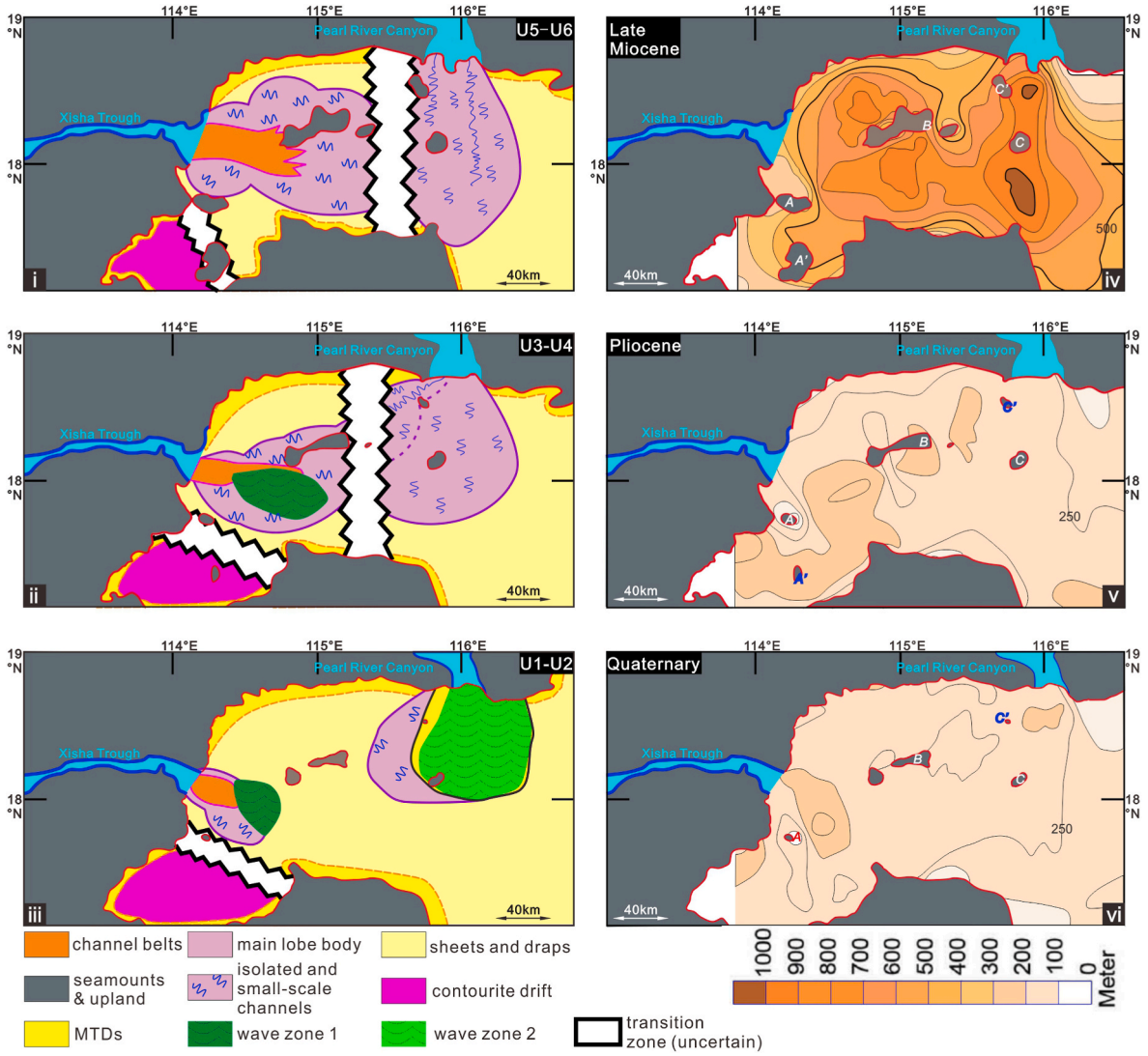

Fig. 15. I to III. Conceptional distribution pattern of the possible deep-water depositional architectural elements within the Northwest Sub-Basin (NWSB) in different units from the Late Miocene onwards, which is based on seismic facies and corresponding interpreted sedimentary facies of basin-floor fan systems since the Late Miocene presented in this study; **IV to VI**. Isopach map showing the decompacted thicknesses of sediments within the NWSB in different units from the Late Miocene onwards (referred from Wu et al., 2018); A, A′, B, C and C′ represent the locations of seamounts that are involved in this study. (NOTE: wavy area 1 represent proposed turbidity sediment-waves, larger scale (about 2 km for wave length, 10 ms TWT for wave height) (Figs. 6g, 8a and 9, 10 and 11); wavy area 2 represent irregular wavy shapes, less scale than wavy area 1 (within 1 km for wave length, about 5 ms TWT for wave height), and these very small scale waves are on-top of and coincides with the mass-transport deposits (MTDs) (Figs. 4, 6h and 12).

the presence of two equally thick depocentres. The Xisha fan seems to have been coarser-grained than the Pearl River fan at this stage, perhaps due to shelf entrapment seawards of the Pearl River sediments in shelf depressions, e.g., the Baiyun Sag and in several slope fans (Pang et al., 2007).

Seismic profiles reveal that within the Xisha fan, possible stacked channel belts are suggested developing at the mouth of the Xisha Trough (Figs. 7, 8a, 9 and 11) and representing the root to upper fan part, whereas similar seismic features appear to be absent at the mouth of the Pearl River Canyon (Figs. 4 and 12). Isolated channels, small scale channels, channel-levee complexes, channel-lobe transition belts and proximal lobes identified on seismic profiles covered the central part of NWSB (Figs. 7–12), composing the upper-middle fan part for both Xisha and Pearl River fans. The boundary between these two fan systems is inferred to be somewhere between the seamounts *s.B* and *s.C/s.C'* (Fig. 15i). However, the nature of this fan inter-digitation is not easily resolved on the 2D seismic lines available. Distal lobes, sheets and drapes identified on seismic profiles make up the lower to distal fan parts and general basin fill, possibly comprising both fine-grained turbidites and hemipelagites. At the foot of slopes surrounding the NWSB, the presence of MTDs (Figs. 7, 8a and 9) is evidence for episodic slope margin collapse. Slope channels (Fig. 8b), distinct from the two principle fan systems, can also contribute thin-bedded turbidites and more dispersed hemipelagic sedimentation across the basin.

Note that during this period the SW corner was partly blocked from sediment supply by the seamounts *s.A/s.A'* (Figs. 4b and 15i). The build-up in this region is inferred as the result of sediment spillover from fine-grained turbidity currents (from the distal fan) interbedded with hemiplegic drapes. These were captured and reworked by the SCS Deep Circulation bottom currents, leading to the contourite drift or terrace (see discussion below).

6.3.2. *Pliocene*

During the Pliocene, the sedimentary budget of the NWSB approximately halved (~1280 km^3/My, ~5.8 cm/ky of the sedimentation rate, Wu et al., 2018). The depocentres seemed shifting to the SW side of

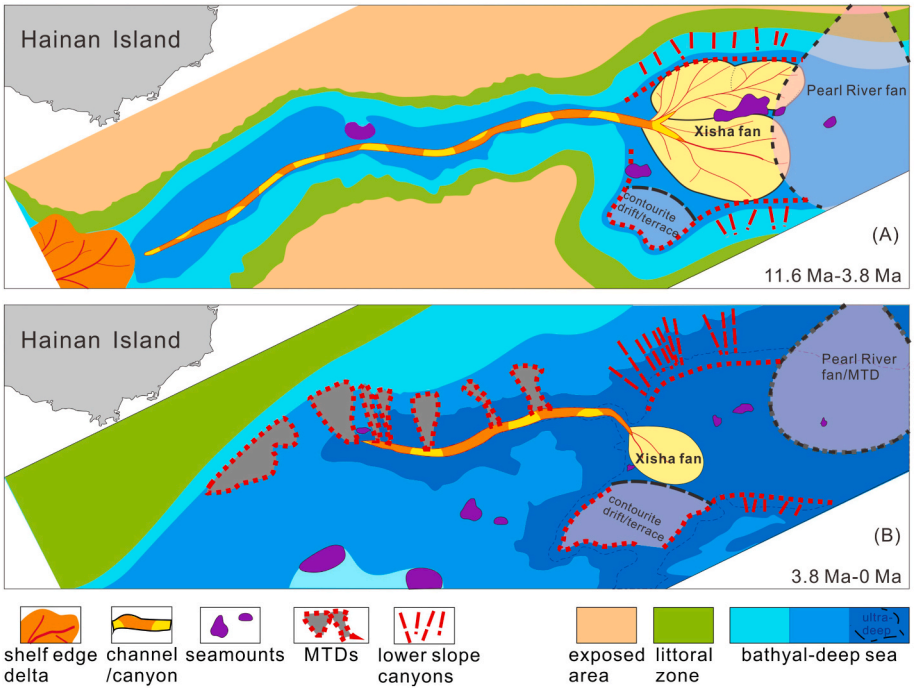

Fig. 16. The possible development pattern of the submarine fan systems in the Northwest Sub-Basin, South China Sea from 11.6 to 3.8 Ma (**A**) and from 3.8 to 0 Ma (**B**) (improved on (Chen et al., 2020)).

seamount *s.B* and the NW side of seamounts *s.C/s.C'*, respectively, for the Xisha and Pearl River fans (Fig. 15iv–vi), with inter-digitation somewhere along the eastern edge of *s.B* (Figs. 15i–iii). Sediment supply to the Xisha fan is suggested decreasing markedly. At the mouth of Xisha Trough, on the upper fan, seismic features interpreted as stacked channel belts were replaced by stacked isolated channels. A smaller number of isolated channels (compared to U5 and U6), together with widely developed channel-levee complexes, small-scale channels and proximal lobes, built up the major upper-middle fan part. The areal extent of basin-floor sheets and drapes was correspondingly enlarged. MTDs derived from the northern slopes as well as from the Xisha Trough walls could be transported eastwards within the Central Canyon, while sediment supply from the further western source was absent (He et al., 2011; Su et al., 2014; Shang et al., 2015).

The Pearl River fan should also diminish in size during this period, building up with small-scale channels, lobe deposits, sheets and drapes (Figs. 4 and 12). Although its total area seemed remaining more or less the same as that during the Late Miocene, the upper-middle fan part was suggested restraining within the area between seamounts *s.B* and *s.C/s.C'* (Fig. 15ii). Such a reduction of the upper-middle fan part in scale might be related to a decrease in size of the upper shelf delta (Fig. 1b), as well as a move of the shelf-break further away from the Pearl River mouth than during the Late Miocene and before (Mao, 2015; Chen et al., 2020).

6.3.3. *Quaternary*

During the Quaternary, the sedimentary budget of the NWSB more or less doubled again to ~2250 km^3/My (~10.1 cm/ky of the sedimentation rate, Wu et al., 2018). For the Xisha fan, however, the western sediment supply should have drastically diminished. MTDs from the northern slope of the Central Canyon should be insufficient to fill up Xisha Trough (Fig. 14c), and a very limited amount of sediment could be therefore delivered into the NWSB. Only a small Xisha fan (the main lobe area smaller than 3500 km^2) could continue to develop, with a few small-scale channels and widely developed sheets and drapes (Figs. 4, 7–12 and 15iii). Here, it is speculated that the apparent sediment deficit from the west coupled with a doubling of the overall sediment budget, indicates an increase in supply from elsewhere. This increase might be in part from the Pearl River Canyon source and growth of the Pearl River basin-floor fan, and in part from slope channels and MTD transport (Fig. 15iii). Sun et al. (2018a) estimated that the total volume of these MTDs imaged on seismic data reached over 600 km^3 in the NSWB. Such enhanced sediment supply through the Pearl River Canyon and northern slope region is believed to be related to continental erosion and sediment transportation under an intensified Asian summer monsoon and glacial-interglacial climate fluctuations (Wu et al., 2018).

Thus, the changing of average sedimentation rate over the NWSB in three periods (~12 cm/ky during the Late Miocene, ~5.8 cm/ky during the Pliocene and ~10.1 cm/ky during the Quaternary) could be attributed to the comprehensive impact of the continuously reduced sediment input from the west and the first reduced then increased sediment input from the northeast. In-depth quantitative discussion for their corresponding decisive control on the basin-floor fans' evolution, however, remains controversial. Future work such as the historical sediment composition comparison between the Pearl River Fan and the Pearl River Canyon and drilling on the Xisha Fan may significantly advance the above research, which is beyond the scope of this paper.

Over the elevated part in the SW region of NWSB, a thick accumulation of very long and long HARPs and M-LARPs throughout U1 to U6 (Fig. 4b) may coincide with deep-water environmental changes that significantly enhanced deep-sea circulation within the northern SCS since the Late Miocene (Xie et al., 2011; Gong et al., 2013; Chen et al., 2014; Sun et al., 2017). Liang et al. (2019) suggested that the deep-sea circulation flowing from east to west along the northern margins of the SCS may have been increasing since the Late Miocene. Drift deposits accumulated widely along the Dongsha and Yitong slope during this period (Chen et al., 2013, 2014, (Chen et al., 2019)). Chen et al. (2016) reported that with the impacts of deep-water tidal and geostrophic currents, some of the present-day cyclonic SCS Deep Water currents can sweep the SW slope margin of the NWSB with current velocities exceeding 15 cm/s. These velocities would enable erosion of the seabed, as well as the capture and dispersion of fine-grained turbidity current plumes and hemipelagic sediments from the slope margin towards the SW corner of the basin. Accumulation of contourite deposition is

possible when the current velocity decreases and/or bottom currents are ponded (Hernández-Molina et al., 2008). However, detailed description and discussion of these contourites are beyond the scope of this study but will be continued in future studies.

7. Conclusions

Based on seismic facies interpretation of 2D seismic reflection data, this study has documented the existence and evolution of two possible large-scale basin-floor fan systems (total thickness over 1.2 s TWT), which have developed since the Late Miocene (11.6 Ma) in the NWSB of the SCS. They have been named as the *Xisha* and *Pearl River basin-floor fan systems*, and the nature and distribution of their individual architectural elements based on seismic profile analysis have been investigated. The Xisha fan may reach its largest extent during the Late Miocene, while the Pearl River fan should be most active during the Late Miocene and Quaternary. Within these basin-floor fan systems, the upper to middle fan parts are suggested to comprise stacked channel belts/isolated channels, channel-levee complexes and proximal lobes, whereas the middle-lower and terminal parts of the fan comprise small-scale channels, (distal) lobe deposits, basin sheets and drapes. The surrounding basin slope, especially to the north, shows numerous MTDs interbedded with background slope sediments. The SW corner of the NWSB appears to have been influenced by bottom currents building a contourite drift/terrace.

Tentative reconstructions show that the development of the Late Miocene-Pliocene Xisha basin-floor fan was mainly controlled by sediment supply. During the Late Miocene, abundant sediments are believed to have originated from SE Asia and be delivered to the NWSB through the Central Canyon/Xisha Trough. From the middle Pliocene onwards, however, this basin-floor fan system may greatly diminish in size, due to the possible sharp decrease of sediment supply from the Central Canyon. Supply of sediments from the Pearl River and northern slope may increase through the Pliocene and into the Quaternary. The results of this study propose a possibility of association between the evolution of the Central Canyon and Xisha fan, which may further add to our understanding of the source to sink systems feeding marginal oceanic basins such as the SCS.

CRediT authorship contribution statement

Hui Chen: Conceptualization, Writing - original draft, Methodology, Software, Investigation, Project administration, Funding acquisition. **Dorrik A.V. Stow:** Conceptualization, Writing - review & editing, Supervision. **Xinong Xie:** Conceptualization, Resources, Writing - review & editing, Supervision, Project administration, Funding acquisition. **Jianye Ren:** Resources, Writing - review & editing, Funding acquisition. **Kainan Mao:** Investigation. **Ya Gao:** Software, Investigation. **Beichen Chen:** Software, Investigation. **Wenyan Zhang:** Writing - review & editing. **Thomas Vandorpe:** Methodology, Software, Writing - review & editing. **David Van Rooij:** Conceptualization, Writing - review & editing.

Declaration of competing interest

The authors declare that they have no known competing financial interests or personal relationships that could have appeared to influence the work reported in this paper.

Acknowledgements

The study was supported by the National Natural Science Foundation of China (Nos. 41976067, 41830537, 91528301), the China-ASEAN Maritime Cooperation Fund Project (12120100500017001), the Programme of Introducing Talents of Discipline to Universities (No. B14031), and the Fundamental Research Funds for the Central Universities, China University of Geosciences (Wuhan) (Nos. CUG170659). We would like to acknowledge the China National Offshore Oil Corporation for providing geophysical data. We thank Ben Kneller, Tilmann Schwenk and Khurram Shahzad for their pre-review and review comments as well as constructive suggestions, comments, which significantly improved the manuscript.

Appendix A. Supplementary data

Supplementary data to this article can be found online at https://doi.org/10.1016/j.marpetgeo.2020.104803.

References

Badalini, G., Kneller, B., Winker, C.D., 2000. Architecture and processes in late Pleistocene brazos-trinity turbidite systems. In: Weimer, P., Slatt, R.M., Coleman, J., Rosen, N.C., Nelson, H., Bouma, A.H., Styzen, M.J., Lawrence, D.T. (Eds.), Gulf Coast Section Society of Economic Paleontologists and Mineralogists 20th Annual Research Conference, pp. 16–33.

Bastia, R., Das, S., Radhakrishna, M., 2010. Pre- and post-collisional depositional history in the upper and middle Bengal fan and evaluation of deep-water reservoir potential along the northeast Continental Margin of India. Mar. Petrol. Geol. 27, 2051–2061.

Bouma, A.H., Coleman, J.M., the Leg 96 Scientific Party, 1985. Seismic stratigraphy and sedimentology of Leg 96 drilling on the Mississippi Fan. GCAGS Transactions 35, 327–331.

Bouma, A.H., 2000. Coarse-grained and fine-grained turbidite systems as end member models: applicability and dangers. Mar. Petrol. Geol. 17, 137–143.

Bouma, A.H., 2001. Fine-grained submarine fans as possible recorders of long- and short-term climatic changes. Global Planet. Change 28, 85–91.

Brooks, H.L., Hodgson, D.M., Brunt, R.L., Peakall, J., Hofstra, M., Flint, S.S., 2018. Deep-water channel-lobe transition zone dynamics: processes and depositional architecture, an example from the Karoo Basin, South Africa. GSA Bull. 130, 1723–1746.

Browne, G.H., King, P.R., Higgs, K.E., Slatt, R.M., 2005. Grain-size characteristics for distinguishing basin floor fan and slope fan depositional settings: outcrop and subsurface examples from the late Miocene Mount Messenger Formation, New Zealand. N. Z. J. Geol. Geophys. 48 (2), 213–227.

Cao, L.C., Jiang, T., Wang, Z.F., Zhang, Y.Z., Sun, H., 2015. Provenance of upper Miocene sediments in the Yinggehai and Qiongdongnan basins, northwestern south China sea: evidence from REE, heavy minerals and zircon U-Pb ages. Mar. Geol. 361, 136–146.

Cartigny, M.J.B., Postma, G., van den Berg, J.H., Mastbergen, D.R., 2011. A comparative study of sediment waves and cyclic steps based on geometries, internal structures and numerical modeling. Mar. Geol. 280, 40–56.

Clift, P.D., Sun, Z., 2006. The sedimentary and tectonic evolution of the Yinggehai–Song Hong basin and the southern Hainan margin, South China Sea: Implications for Tibetan uplift and monsoon intensification. J. Geophys. Res. Solid Earth 111, B6.

Cui, Y., Shao, L., Qiao, P., Pei, J., Zhang, D., Tran, H., 2018. Upper miocene–pliocene provenance evolution of the central canyon in northwestern south China sea. Mar. Geophys. Res. 40 (2), 223–235.

Chen, H., Xie, X., Guo, J.L., Su, M., Zong, K.Q., Shang, F., Huang, W., Wang, W., Shang, Z. L., 2015. Provenance of central canyon in Qiongdongnan basin as evidenced by detrital zircon U-Pb study of upper Miocene sandstones. Sci. China Earth Sci. 58, 1337–1349.

Chen, H., Xie, X., Mao, K., He, Y., Su, M., Zhang, W., 2020. Depositional characteristics and formation mechanisms of deep-water canyon systems along the northern South China Sea margin. J. Earth Sci. 31 (4), 808–819.

Chen, H., Xie, X., Van Rooij, D., Vandorpe, T., Huang, L., Guo, L., Su, M., 2013. Depositional characteristics and spatial distribution of deep-water sedimentary systems on the northwestern middle-lower slope of the Northwest Sub-Basin, South China Sea. Mar. Geophys. Res. 34, 239–257.

Chen, H., Xie, X., Van Rooij, D., Vandorpe, T., Su, M., Wang, D., 2014. Depositional characteristics and processes of alongslope currents related to aseamount on the northwestern margin of the Northwest Sub-Basin, South China Sea. Mar. Geol. 355, 36–53.

Chen, H., Xie, X., Zhang, W., Shu, Y., Wang, D., Vandorpe, T., Van Rooij, D., 2016. Deep-water sedimentary systems and their relationship with bottom currents at the intersection of Xisha Trough and Northwest Sub-Basin, South China Sea. Mar. Geol. 378, 101–113.

Chen, J.S., Xu, S.C., Sang, J.Y., 1994. The depositional characteristics and oil potential of paleo-Pearl River delta systems in the Pearl River Mouth Basin, South China Sea. Tectonophysics 235, 1–11.

Chen, H., Zhang, W., Xie, X., Ren, J., 2019. Sediment dynamics driven by contour currents and mesoscale eddies along continental slope: A case study of the northern South China Sea. Mar. Geol. 409, 48–66.

Clark, J.D., Pickering, K.T., 1996. Submarine Channels: Processes and Architecture. Vallis Press, London, pp. 1–231.

de Haas, H., van Weering, T.C.E., Stoker, M.S., 2003. Development of a sediment drift: Feni drift, NE Atlantic margin. In: Mienert, J., Weaver, P. (Eds.), European Margin Sediment Dynamics: Side-Scan Sonar and Seismic Images. Springer Berlin Heidelberg, Berlin, Heidelberg, pp. 197–201.

Deptuck, M.E., Piper, D.J.W., Savoye, B., Gervais, A., 2008. Dimensions and architecture of late Pleistocene submarine lobes off the northern margin of East Corsica. Sedimentology 55, 869–898.
Deptuck, M.E., Steffens, G.S., Barton, M., Pirmez, C., 2003. Architecture and evolution of upper fan channel-belts on the Niger Delta slope and in the Arabian Sea. Mar. Petrol. Geol. 20, 649–676.
Deptuck, M.E., Sylvester, Zoltán, 2018. Submarine fans and their channels, levees, and lobes. In: Micallef, A., Krastel, S., Savini, A. (Eds.), Submarine Geomorphology. Springer International Publishing, Cham, pp. 273–300.
Ding, W., Li, J., Li, J., Fang, Y., Tang, Y., 2013. Morphotectonics and evolutionary controls on the Pearl River canyon system, south China sea. Mar. Geophys. Res. 34, 221–238.
Ding, W., Li, M., Zhao, L., Ruan, A., Wu, Z., 2009. Cenozoic tectono-sedimentary characteristics and extension model of the north-west sub-basin, south China sea. Earth Sci. Front. 2, 147–156.
Faugères, J.C., Stow, D.A., Imbert, P., Viana, A., 1999. Mar. Geol. 162, 1–38.
Flood, R.D., Piper, D.J.W., 1997. Amazon Fan sedimentation: the relationship to equatorial climate change, continental denudation, and sea-level fluctuations. In: Flood, R.D., Piper, D.J.W., Klaus, A., Peterson, L.C. (Eds.), Proceedings of the Ocean Drilling Program, Scientific Results 155. Texas A&M University, Galveston, pp. 653–675.
Gamberi, F., Rovere, M., 2011. Architecture of a modern transient slope fan (Villafranca fan, Gioia basin–Southeastern Tyrrhenian Sea). Sediment. Geol. 236 (3), 211–225.
Gan, J., Li, H., Curchitser, E., Haidvogel, D., 2006. Modeling South China Sea circulation: response to seasonal forcing regimes. J. Geophys. Res. Oceans 111, C06034.
Gervais, A., Mulder, T., Savoye, B., Gonthier, E., 2006. Sediment distribution and evolution of sedimentary processes in a small sandy turbidite system (Golo system, Mediterranean Sea): implications for various geometries based on core framework. Geo Mar. Lett. 26 (6), 373–395.
Gong, C., Wang, Y., Zhu, W., Li, W., Xu, Q., Zhang, J., 2011. The central submarine canyon in the Qiongdongnan basin, northwestern south China sea: architecture, sequence stratigraphy, and depositional processes. Mar. Petrol. Geol. 28, 1690–1702.
Gong, C., Wang, Y., Zhu, W., Li, W., Xu, Q., 2013. Upper Miocene to quaternary unidirectionally migrating deep-water channels in the Pearl River Mouth Basin, northern South China sea. AAPG (Am. Assoc. Pet. Geol.) Bull. 97, 285–308.
Hansen, L.A.S., Callow, R.H.T., Kane, I.A., Gamberi, F., Rovere, M., Cronin, B.T., Kneller, B.C., 2015. Genesis and character of thin-bedded turbidites associated with submarine channels. Mar. Petrol. Geol. 67, 852–879.
Haq, B.U., Hardenbol, J., Vail, P.R., 1987. Chronology of fluctuating sea levels since the Triassic. Science 235, 1156–1167.
He, Y., Xie, X., Kneller, B.C., Wang, Z., Li, X., 2013. Architecture and controlling factors of canyon fills on the shelf margin in the Qiongdongnan Basin, northern South China Sea. Mar. Petrol. Geol. 41, 264–276.
He, Y., Xie, X., Lu, Y., Li, J., Zhang, C., Jiang, T., Su, M., 2011. Architecture and characteristics of mass-transport deposits (MTDs) in Qiongdongnan basin in northern South China sea. Earth Sci. J. China Univ. Geosci. 36, 905–913.
Hernández-Molina, F.J., Maldonado, A., Stow, D.A.V., 2008. Chapter 18 abyssal plain contourites. In: Rebesco, M., Camerlenghi, A. (Eds.), Contourites. Elsevier, Amsterdam, pp. 345–378.
Hessler, A.M., Fildani, A., 2019. Deep-sea fans: tapping into Earth's changing landscapes. J. Sediment. Res. 89, 1171–1179.
Hiscott, R.N., Hall, F.R., Pirmez, C., 1997. Turbidity-current overspill from the Amazon channel: texture of the silt/sand load, paleoflow from anisotropy of magnetic susceptibility and implications for flow processes. In: Flood, R.D., Piper, D.J.W., Klaus, A., Peterson, L.C. (Eds.), Proceedings of the Ocean Drilling Program, Scientific Results 155. Texas A&M University, Galveston, pp. 53–78.
Huang, W., Xie, X.N., He, Y.L., Wu, J.F., Zhao, Z.G., Wang, X.J., 2015. Evolution and reservoir prediction of Yinggehai formation in western central canyon in Qiongdongnan basin. Acta Sedimentol. Sin. 33 (4), 809–816.
Janocko, M., Nemec, W., Henriksen, S., Warchoł, M., 2013. The diversity of deep-water sinuous channel belts and slope valley-fill complexes. Mar. Petrol. Geol. 41, 7–34.
Jian, Z., Larsen, H.C., Alvarez Zarikian, C.A., the Expedition 368 Scientists, 2018. Expedition 368 Preliminary Report: South China Sea Rifted Margin. International Ocean Discovery Program.
Jiang, T., Cao, L., Xie, X., Wang, Z., Li, X., Zhang, Y., Zhang, D., Sun, H., 2015. Insights from heavy minerals and zircon U–Pb ages into the middle Miocene–Pliocene provenance evolution of the Yinggehai Basin, northwestern South China Sea. Sediment. Geol. 327, 32–42.
Johnson, S.D., Flint, S., Hinds, D., De Ville Wickens, H., 2001. Anatomy, geometry and sequence stratigraphy of basin floor to slope turbidite systems, Tanqua Karoo, South Africa. Sedimentology 48, 987–1023.
Kane, I.A., Hodgson, D.M., 2011. Sedimentological criteria to differentiate submarine channel levee subenvironments: exhumed examples from the rosario Fm. (Upper Cretaceous) of Baja California, Mexico, and the Fort Brown Fm. (Permian), Karoo basin, S. Africa. Mar. Petrol. Geol. 28, 807–823.
Kang, B., Xie, X., Cui, T., 2014. Numerical approach for thermal history modelling in multi-episodic rifting basins. Earth Sci. J. China Univ. Geosci. 25 (3), 519–528.
Kastens, K.A., Shor, A.N., 1986. Evolution of a channel meander on the Mississippi Fan. Mar. Geol. 71, 165–175.
King, P.R., Browne, G.H., Slatt, R.M., Weimer, P., Bouma, A., Perkins, B., 1994. Sequence architecture of exposed late Miocene basin floor fan and channel-levee complexes (Mount Messenger Formation), Taranaki Basin, New Zealand. Submarine fans and turbidite systems: sequence stratigraphy, reservoir architecture and production characteristics. In: Gulf of Mexico and International: Proceedings Gulf Coast Section Society of Economic Paleontologists and Mineralogists Foundation Fifteenth Annual Research Conference, GCS017, pp. 177–192.
Kneller, B.C., McCaffrey, W.D., 1995. Modelling the Effects of Salt-Induced Topography on Deposition from Turbidity Currents. Society of Economic Palaeontologists and Mineralogists Gulf Coast Section, pp. 137–145.
Kneller, B.C., Martinsen, O.J., Mccaffrey, B., 2009. External Controls on Deep-Water Depositional Systems, vol. 92. SEPM Special Publication, pp. 1–403.
Knudson, K.P., Hendy, I.L., 2009. Climatic influences on sediment deposition and turbidite frequency in the Nitinat Fan, British Columbia. Mar. Geol. 262, 29–38.
Kolla, V., 2007. A review of sinuous channel avulsion patterns in some major deep-sea fans and factors controlling them. Mar. Petrol. Geol. 24 (6), 450–469.
Kolla, V., Posamentier, H.W., Wood, L.J., 2007. Deep-water and fluvial sinuous channels: characteristics, similarities and dissimilarities, and modes of formation. Mar. Petrol. Geol. 24 (6–9), 388–405.
Kusznir, N.J., Roberts, A.M., Morley, C.K., 1995. Forward and reverse modelling of rift basin formation. Geol. Soc. Lond. Spec. Publ. 80, 33–56.
Liang, C., Xie, X.N., Wang, H., Chen, H., Shi, G.Z., Zhong, G.J., Liu, E.T., Sun, M., Yi, H., 2019. Depositional evolution of sediment drifts inside intra-slope basins on the lower southeastern slope of the Dongsha Islands (South China Sea) and their paleoceanographic implications. Geo Mar. Lett. 39 (2), 101–116.
Lan, J., Zhang, N., Wang, Y., 2013. On the dynamics of the South China Sea deep circulation. J. Geophys. Res. Oceans 118, 1206–1210.
Larsen, H.C., Mohn, G., Nirrengarten, M., Sun, Z., Stock, J., Jian, Z., Klaus, A., Alvarez-Zarikian, C.A., Boaga, J., Bowden, S.A., Briais, A., Chen, Y., Cukur, D., Dadd, K., Ding, W., Dorais, M., Ferré, E.C., Ferreira, F., Furusawa, A., Gewecke, A., Hinojosa, J., Höfig, T.W., Hsiung, K.H., Huang, B., Huang, E., Huang, X.L., Jiang, S., Jin, H., Johnson, B.G., Kurzawski, R.M., Lei, C., Li, B., Li, L., Li, Y., Lin, J., Liu, C., Liu, C., Liu, Z., Luna, A.J., Lupi, C., McCarthy, A., Ningthoujam, L., Osono, N., Peate, D.W., Persaud, P., Qiu, N., Robinson, C., Satolli, S., Sauermilch, I., Schindlbeck, J.C., Skinner, S., Straub, S., Su, X., Su, C., Tian, L., van der Zwan, F.M., Wan, S., Wu, H., Xiang, R., Yadav, R., Yi, L., Yu, P.S., Zhang, C., Zhang, J., Zhang, Y., Zhao, N., Zhong, G., Zhong, L., 2018. Rapid transition from continental breakup to igneous oceanic crust in the South China Sea. Nat. Geosci. 11, 782–789.
Leloup, P.H., Lacassin, R., Tapponnier, P., Schärer, U., Zhong, D., Liu, X., Zhang, L., Ji, S., Trinh, P.T., 1995. The Ailao Shan-Red River shear zone (Yunnan, China), tertiary transform boundary of Indochina. Tectonophysics 251, 3–84.
Li, C., Lv, C., Chen, G., Zhang, G., Ma, M., Shen, H., Zhao, Z., Guo, S., 2017. Source and sink characteristics of the continental slope-parallel central canyon in the Qiongdongnan basin on the northern margin of the south China sea. J. Asian Earth Sci. 134, 1–12.
Li, H., Wang, Y., Zhu, W., Xu, Q., He, Y., Tang, W., Zhuo, H., Wang, D., Wu, J., Li, D., 2013. Seismic characteristics and processes of the Plio-Quaternary unidirectionally migrating channels and contourites in the northern slope of the South China Sea. Mar. Petrol. Geol. 43, 370–380.
Li, Q., Zhong, G., Tian, J., 2009. Stratigraphy and sea level changes. In: Wang, P., Li, Q. (Eds.), The South China Sea. Springer Netherlands, Berlin, pp. 75–170.
Liu, B.J., Pang, X., Yan, C.Z., Liu, J., Lian, S.Y., He, M., Shen, J., 2011. Evolution of the Oligocene-Miocene shelf slope-break zone in the Baiyun deep-water area of the Pearl River Mouth Basin and its significance in oil-gas exploration. Acta Pet. Sin. 32 (2), 234–242.
Liu, R., Zhou, J.Y., Zhang, L., Liu, X.F., Yi, H., Liao, J.F., 2012. Provenance supply model and exploration prospect of the northwestern sub-basin, south China sea. Acta Geol. Sin. 86 (11), 1826–1832.
Lopez, M., 2001. Architecture and depositional pattern of the Quaternary deep-sea fan of the Amazon. Mar. Petrol. Geol. 18 (4), 479–486.
Lüdmann, T., Wong, H.K., Berglar, K., 2005. Upward flow of north pacific deep water in the northern South China sea as deduced from the occurrence of drift sediments. Geophys. Res. Lett. 32, L05614.
Madof, A.S., Christie-Blick, N., Anders, M.H., 2009. Stratigraphic controls on a salt-withdrawal intraslope minibasin, north-central Green Canyon, Gulf of Mexico: implications for misinterpreting sea level change. AAPG (Am. Assoc. Pet. Geol.) Bull. 93, 535–561.
Mao, K., 2015. Internal Architectures and Depositional Model of the Pearl River Submarine Canyon System. PhD thesis. China University of Geosciences, Wuhan, pp. 1–116.
Mao, K., Xie, X., Xie, Y., Ren, J., Chen, H., 2015. Post-rift tectonic reactivation and its effect on deep-water deposits in the Qiongdongnan Basin, northwestern South China Sea. Mar. Geophys. Res. 36 (2), 227–242.
Mayall, M., Jones, E., Casey, M., 2006. Turbidite channel reservoirs-Key elements in facies prediction and effective development. Mar. Petrol. Geol. 23 (8), 821–841.
Mayall, M., Stewart, I., 2000. The architecture of turbidite slope channels. Global deep-water reservoirs: Gulf Coast Section SEPM Foundation 20th Annual Bob F. Perkins Research Conference 578–586.
Mulder, T., 2011. Chapter 2 - gravity processes and deposits on continental slope, rise and abyssal plains. In: Hüneke, H., Mulder, T. (Eds.), Deep-Sea Sediments. Elsevier, Amsterdam, pp. 25–148.
Mulder, T., Etienne, S., 2010. Lobes in deep-sea turbidite systems: state of the art. Sediment. Geol. 229 (3), 75–80.
Mutti, E., 1985. Turbidite systems and their relations to depositional sequences. In: Zuffa, G.G. (Ed.), Provenance of Arenites. NATOASI Series. D. . Reidel Publishing Co., pp. 65–93
Mutti, E., Normark, W.R., 1987. Comparing examples of modern and ancient turbidite systems: problems and concepts. In: Legget, J.K., Zuffa, G.G. (Eds.), Marine Clastic Sedimentology. Graham and Trotman, London, pp. 1–38.
Mutti, E., Lucchi, Ricci, 1972. Turbidites of the northern Apennines: introduction to facies analysis. Int. Geol. Rev. 20, 125–166.

Nilsen, T.H., 1980. Modern and ancient submarine fans: discussion of papers by Walker and Normark. AAPG (Am. Assoc. Pet. Geol.) Bull. 64 (7), 1094–1101.
Normark, W.R., 1970. Growth patterns of deep-sea fans. AAPG (Am. Assoc. Pet. Geol.) Bull. 54 (11), 2170–2195.
Normark, W.R., 1978. Fan valleys, channels, and depositional lobes on modern submarine Fans: characters for recognition of sandy turbidite environments. AAPG Bull. 62 (6), 912–931.
Normark, W.R., Piper, D.J.W., Sliter, R., 2006. Sea-level and tectonic control of middle to late Pleistocene turbidite systems in Santa Monica Basin, offshore California. Sedimentology 53, 867–897.
Normark, W.R., Posamentier, H., Mutti, E., 1993. Turbidite systems: state of the art and future directions. Rev. Geophys. 31, 91.
Pang, X., Chen, C., Peng, D., Zhu, M., Shu, Y., He, M., Shen, J., Liu, B., 2007. Sequence stratigraphy of deep-water fan system of Pearl River, south China sea. Earth Sci. Front. 14 (1), 220–229.
Pang, X., Chen, C., Shi, H., Shu, Y., Shao, L., He, M., Shen, J., 2005. Response between relative sea-level change and the Pearl River deep-water fan system in the South China Sea. Earth Sci. Front. 12 (3), 167–177.
Pickering, K.T., Clark, J.D., Smith, R.D.A., Hiscott, R.N., Ricci Lucchi, F., Kenyon, N.H., 1995. Architectural element analysis of turbidite systems, and selected topical problems for sand-prone deep-water systems. In: Pickering, K.T., Hiscott, R.N., Kenyon, N.H., Ricci Lucchi, F., Smith, R.D.A. (Eds.), Atlas of Deep-Water Environments: Architectural Style in Turbidite Systems. Springer Netherlands, Dordrecht, pp. 1–10.
Pickering, K.T., Hiscott, R.N., 2015. Deep Marine Systems: Processes, Deposits, Environments, Tectonics and Sedimentation. AGU Earth Science, pp. 1–672.
Piper, D.J.W., Hiscott, R.N., Normark, W.R., 1999. Outcrop-scale acoustic facies analysis and latest Quaternary development of Hueneme and Dume submarine fans, offshore California. Sedimentology 46 (1), 47–78.
Piper, D.J.W., Normark, W.R., 2001. Sandy fans-from Amazon to Hueneme and beyond. AAPG (Am. Assoc. Pet. Geol.) Bull. 85 (8), 1407–1438.
Piper, D.J.W., Pirmez, C., Manley, P.L., Long, D., Flood, R.D., Normark, W.R., Showers, W., 1997. Mass-transport deposits of the Amazon FanFlood, R.D., Piper, D. J., Klaus, A., Peterson, L.C. (Eds.), In: Scientific Results, Amazon Fan. Proceedings of the Ocean Drilling Program, 155. College Station, TX, pp. 109–146.
Pirmez, C., Beaubouef, R.F., Friedman, S.J., Morig, D.C., 2000. Equilibrium profile and baselevel in submarine channels: examples from late Pleistocene systems and implications for the architecture of deepwater reservoirs. In: Weimer, P., Slatt, R.M., Coleman, J., Rosen, N.C., Nelson, H., Bouma, A.H., Styzen, M.J., Lawrence, D.T. (Eds.), Gulf Coast Section Society of Economic Paleontologists and Mineralogists 20th Annual Research Conference, pp. 782–805.
Pirmez, C., Flood, R.D., 1995. Morphology and structure of Amazon channel. In: Flood, R.D., Piper, D.J.W., Klaus, A. (Eds.), Proceedings of the Ocean Drilling Program, Initial Report. Texas A&M University, Galveston, pp. 23–45.
Posamentier, H.W., 2003. Depositional elements associated with a basin floor channel-levee system: case study from the Gulf of Mexico. Mar. Petrol. Geol. 20 (s6–8), 677–690.
Posamentier, W., Jervey, M.T., Vail, P.R., 1988. Eustatic controls on clastic deposition. In: Wilgus, C.K., Hastings, B.S., Posamentier, H.S., Van Wagoner, J., Ross, C.K., Kendell, C.G. (Eds.), Sea-level Changes: an Integrated Approach. SPEM Special Publicatoin. 42. Soc. Econ. Paleontol. Mineral., Tulsa, OK, pp. 69–154.
Prather, B.E., 2003. Controls on reservoir distribution, architecture and stratigraphic trapping in slope setting. Mar. Petrol. Geol. 20, 529–545.
Qin, G.Q., 1996. Application of micropaleontology to the sequence stratigraphic studies of late Cenozoic in the Zhujiang River mouth basin. Mar. Geol. Quat. Geol. 16 (4), 1–18.
Reading, H.G., Richards, M., 1994. Turbidite systems in deep-water basin margins classified by grain size and feeder system. AAPG (Am. Assoc. Pet. Geol.) Bull. 78 (5), 792–822.
Ru, K., Pigott, J.D., 1986. Episodic rifting and subsidence in the south China sea. AAPG (Am. Assoc. Pet. Geol.) Bull. 70, 1136–1155.
Saller, A.H., Noah, J.T., Ruzuar, A.P., Schneider, R., 2004. Linked lowstand delta to basin-floor fan deposition, offshore Indonesia: an analog for deep-water reservoir systems. AAPG (Am. Assoc. Pet. Geol.) Bull. 88 (1), 21–46.
Schwenk, T., Spieß, V., Breitzke, M., Hübscher, C., 2005. The architecture and evolution of the Middle Bengal Fan in vicinity of the active channel-levee system imaged by high-resolution seismic data. Mar. Petrol. Geol. 22 (5), 637–656.
Shao, L., Cui, Y., Stattegger, K., Zhu, W., Qiao, P., Zhao, Z., 2019. Drainage control of Eocene to Miocene sedimentary records in the southeastern margin of Eurasian Plate. GSA Bull. 131 (3–4), 461–478.
Shao, L., Li, X., Geng, J., Pang, X., Lei, Y., Qiao, P., Wang, L., Wang, H., 2007. Deep water bottom current deposition in the northern South China Sea. Sci. China Earth Sci. 50, 1060–1066.
Shang, Z., Xie, X., Li, X., Zhang, D., He, Y., Yang, X., Cui, M., 2015. Difference in full-filled time and its controlling factors in the central canyon of the Qiongdongnan basin. Acta Oceanol. Sin. 34 (10), 81–89.
Shanmugam, G., 2006. Deep-water Processes and Facies Models: Implications for Sandstone Petroleum Reservoirs. Elsevier B.V., Berlin, pp. 1–496.
Shanmugam, G., Moiola, R., 1991. Types of submarine fan lobes: models and implications. AAPG (Am. Assoc. Pet. Geol.) Bull. 75, 156–179.
Shanmugam, G., Moiola, R., McPherson, J., O'Connell, S., 1988. Comparison of modern Mississippi fan with selected ancient fans. AAPG (Am. Assoc. Pet. Geol.) Bull. 38, 157–165.
Shu, Y., Xue, H., Wang, D., Chai, F., Xie, Q., Yao, J., Xiao, J., 2014. Meridional overturning circulation in the South China Sea envisioned from the high-resolution global reanalysis data GLBa0.08. J. Geophys. Res. 119, 3012–3028.
Stow, D.A.V., 1981. Fine-grained sediments: terminology. Q. J. Eng. Geol. Hydrogeol. 14, 243–244.
Stow, D.A.V., 1985a. Deep-sea clastics: where are we and where are we going. Geol. Soc. 18 (1), 67–93.
Stow, D.A.V., 1985b. Fine-grained sediments in deep water: an overview of processes and facies models. Geo Mar. Lett. 5, 17–23.
Stow, D.A.V., 1992. Deep-water Turbidite Systems. Blackwell Scientific Publications, Oxford, pp. 1–473.
Stow, D.A.V., Reading, H.G., Collinson, J., 1996. Deep seas. In: Reading, H.G. (Ed.), Sedimentary Environments and Facies, third ed. Blackwell Sci. Publ., pp. 380–442
Stow, D.A.V., Johansson, M., 2000. Deep-water massive sands: nature, origin and hydrocarbon implications. Mar. Petrol. Geol. 17 (2), 145–174.
Stow, D.A.V., Mayall, M., 2000. Deep-water sedimentary systems: new models for the 21st century. Mar. Petrol. Geol. 17 (2), 125–135.
Su, M., 2011. Internal Architectures and Depositional Model of the Central Canyon System since Miocene in Qiongdongnan Basin, Northern South China Sea. China University of Geosciences (Wuhan), Wuhan, pp. 1–138.
Su, M., Li, J., Jiang, T., Tian, S., Zhang, C., Xie, X., 2009. Morphological features and formation mechanism of central canyon in the Qiongdongnan basin, northern South China sea. Mar. Geol. Quat. Geol. 29 (4), 85–93.
Su, M., Xie, X., Li, J., Jiang, T., Zhang, C., He, Y., Tian, S., Zhang, C., 2011. Gravity flow on slope and abyssal systems in the Qiongdongnan basin, northern South China sea. Acta Geol. Sin. 85 (1), 243–253.
Su, M., Xie, X., Xie, Y., Wang, Z., Zhang, C., Jiang, T., He, Y., 2014. The segmentations and the significances of the central canyon system in the Qiongdongnan basin, northern South China sea. J. Asian Earth Sci. 79 (2), 552–563.
Sun, Q.L., Cartwright, J., Lüdmann, T., Wu, S.G., Yao, G.S., 2017. Three-dimensional seismic characterization of a complex sediment drift in the South China Sea: evidence for unsteady flow regime. Sedimentology 64, 832–853.
Sun, Q., Alves, T., Lu, X., Chen, C., Xie, X., 2018a. True volumes of slope failure estimated from a Quaternary mass-transport deposit in the northern South China Sea. Geophys. Res. Lett. 45, 2642–2651.
Sun, Q., Cartwright, J., Xie, X., Lu, X., Yuan, S., Chen, C., 2018b. Reconstruction of repeated Quaternary slope failures in the northern South China Sea. Mar. Geol. 401, 17–35.
Sun, Z., Zhong, Z., Keep, M., Zhou, D., Cai, D., Li, X., Wu, S., Jiang, J., 2009. 3D analogue modeling of the South China Sea: a discussion on breakup pattern. J. Asian Earth Sci. 34 (4), 544–556.
Sun, Z., Zhou, D., Zhong, Z., Xia, B., Qiu, X., Zeng, Z., Jiang, J., 2006. Research on the dynamics of the South China Sea opening: evidence from analogue modelling. Sci. China Earth Sci. 49, 1053–1069.
Taylor, B., Hayes, D.E., 1983. Origin and history of the south China sea basin. In: Hayes, D.E. (Ed.), The Tectonic and Geologic Evolution of Southeast Asian Seas and Islands: Part 2. Washington D.C., USA, vol. 27. American Geophysical Union, pp. 23–56.
van Hoang, L., Wu, F.Y., Clift, P.D., 2009. Evaluating the evolution of the Red River system based on in situ U-Pb dating and Hf isotope analysis of zircons. G-cubed 10 (11), 292–310.
Van Wagoner, J.C., Posamentier, H.W., Mitchum, R.M., Vail, P.R., Sarg, J.F., Loutit, T.S., Hardenbol, J., 1988. An overview of the fundamentals of sequence stratigraphy and key definitions. In: Wilgus, C.K., Hastings, B.S., Kendall, G.StC., Posamentier, H.W., Ross, C.A., Van Wagoner, J.C. (Eds.), Sea-level Change: an Integrated Approach, vol. 42. SEPM Special Publication, pp. 39–45.
Vittori, J., Morash, A., Savoye, B., Marsset, T., Lopez, M., Droz, L., Cremer, M., 2000. The Quaternary Congo deep-sea fan: preliminary results on reservoir complexity in turbiditic systems using 2D high resolution seismic and multibeam data. In: Weimer, P., Slatt, R.M., Coleman, J., Rosen, N.C., Nelson, H., Bouma, A.H., Styzen, M.J., Lawrence, D.T. (Eds.), Deep-Water Reservoirs of the World: Gulf Coast Section, SEPM 20th Annual Research Conference, pp. 1045–1058.
Walker, R.G., 1978. Deep-water sandstone facies and ancient submarine fans: models for exploration for stratigraphic traps. AAPG (Am. Assoc. Pet. Geol.) Bull. 62 (6), 932–966.
Wang, C., Liang, X., Foster, D.A., Tong, C., Liu, P., Liang, X., Zhang, L., 2019. Linking source and sink: detrital zircon provenance record of drainage systems in Vietnam and the Yinggehai–Song Hong basin, south China sea. GSA Bull. 131 (1–2), 191–204.
Wang, D., Wang, Q., Zhou, W., Cai, S., Li, L., Hong, B., 2013. An analysis of the current deflection around Dongsha Islands in the northern South China Sea. J. Geophys. Res. Oceans 118, 490–501.
Wang, D., Xiao, J., Shu, Y., Xie, Q., Chen, J., Wang, Q., 2016. Progress on deep circulation and meridional overturning circulation in the South China Sea. Sci. China Earth Sci. 59, 1827–1833.
Wang, H., 2007. Sedimentation Processes and its Response in Deep-Water Environment of the Northern Continental Margin, the South China Sea. China University of Petroleum, Beijing, pp. 1–129.
Wang, P., Li, Q., 2009a. Introduction. In: Wang, P., Li, Q. (Eds.), The South China Sea. Springer Netherlands, Berlin, pp. 1–23.
Wang, P., Li, Q., 2009b. Oceanographical and geological background. In: Wang, P., Li, Q. (Eds.), The South China Sea. Springer, Netherlands, pp. 25–73.
Wang, Y.F., Wang, Y.M., Qiang, D., Zhuo, H., Zhou, W., 2012. The early-middle Miocene submarine fan system in the Pearl River Mouth Basin, south China sea. Petrol. Sci. 9 (1), 1–9.
Wang, Y., Xu, Q., Li, D., Han, J., Lü, M., Wang, Y., Li, W., Wang, H., 2011. Late Miocene Red River submarine fan, northwestern south China sea. Chin. Sci. Bull. 56, 1488–1494.
Wang, Z., Jiang, T., Zhang, D., Wang, Y., Zuo, Q., He, W., 2015. Evolution of deep-water sedimentary environments and its implication for hydrocarbon exploration in

Qiongdongnan Basin, northwestern South China Sea. Acta Oceanol. Sin. 34 (4), 1–10.
Watson, M.P., 1981. Submarine fan deposits of the Upper Ordovician Lower Silurian Milliners Arm Formation, New World Island, Newfoundland. D. Phil thesis, University of Oxford, UK.
Wei, K.S., Cui, H.Y., Ye, S.F., Li, D.L., Liu, T.S., Liang, J.S., Yang, G.Z., Wu, L., Zhou, X.Y., Hao, Y.Q., 2001. High-precision sequence stratigraphy in Qiongdongnan basin. J. China Univ. Geosci. 26 (1), 59–66.
Weimer, P., 1989. Sequence stratigraphy of the Mississippi fan (Plio–Pleistocene), Gulf of Mexico. Geo Mar. Lett. 9, 185–272.
Weimer, P., Slatt, R.M., Coleman, J., Rosen, N.C., Nelson, H., Bouma, A.H., Styzen, M.J., Lawrence, D.T., 2000. Deep-water reservoirs of the world. In: Gulf Coast Section SEPM 20th Bob F. Perkins Research Conference, pp. 1–64.
Wu, Y., Ding, W., Clift, P.D., Li, J., Yin, S., Fang, Y., Ding, H., 2018. Sedimentary budget of the Northwest Sub-basin, South China Sea: controlling factors and geological implications. Geol. J. 53 (6), 3082–3092.
Wynn, R.B., Cronin, B.T., Peakall, J., 2007. Sinuous deep-water channels: genesis, geometry and architecture. Mar. Petrol. Geol. 24 (6), 341–387.
Wynn, R.B., Kenyon, N.H., Masson, D.G., Stow, D.A.V., Weaver, P.P.E., 2002. Characterization and recognition of deep-water channel-lobe transition zones. AAPG (Am. Assoc. Pet. Geol.) Bull. 86, 1441–1462.
Wynn, R.B., Stow, D.A.V., 2002. Classification and characterisation of deep-water sediment waves. Mar. Geol. 192, 7–22.
Xie, Q., Xiao, J.G., Wang, D.X., 2013. Analysis of deep-layer and bottom circulations in the South China Sea based on eight quasi-global ocean model outputs. Chin. Sci. Bull. 58, 4000–4011.
Xie, X., Müller, R.D., Ren, J., Jiang, T., Zhang, C., 2008. Stratigraphic architecture and evolution of the continental slope system in offshore Hainan, northern South China Sea. Mar. Geol. 247, 129–144.
Xie, X., Zhang, C., Ren, J., Yao, B., Wan, L., Chen, H., Kang, B., 2011. Effects of distinct tectonic evolutions on hydrocarbon accumulation in northern and southern continental marginal basins of South China Sea. Chin. J. Geophys. 54 (6), 1097–1111.
Xie, Y., Li, X., Fan, C., Tan, J., Liu, K., Lu, Y., Hu, W., Li, H., Wu, J., 2016. The axial channel provenance system and natural gas accumulation of the upper Miocene Huangliu formation in Qiongdongnan basin, south China sea. Petrol. Explor. Dev. 43, 570–578.
Xu, S.H., Xu, G.Q., Yang, J.H., Li, X.G., Hu, L., Cai, C.E., Guo, W., 2013. Reservoir identification and plane distribution research on the deep-water fan of SQ13.8 in the deep-water region, the Baiyun Sag in northern South China Sea: a case study of SF-5. Geoscience 27 (2), 366–372.
Yan, P., Deng, H., Liu, H., Zhang, Z., Jiang, Y., 2006. The temporal and spatial distribution of volcanism in the South China Sea region. J. Asian Earth Sci. 27, 647–659.
Yang, S.Y., Kim, J.W., 2014. Pliocene basin-floor fan sedimentation in the Bay of Bengal (offshore northwest Myanmar). Mar. Petrol. Geol. 49, 45–58.
Yin, S., Li, J., Ding, W., Sawyer, D.E., Wu, Z., Tang, Y., 2018. Sedimentary filling characteristics of the South China Sea oceanic basin, with links to tectonic activity during and after seafloor spreading. Int. Geol. Rev. 1–21.
Yin, S., Hernández-Molina, F.J., Zhang, W., Li, J., Wang, L., Ding, W., Ding, W., 2019. The influence of oceanographic processes on contourite features: a multidisciplinary study of the northern South China Sea. Mar. Geol. 415, 105967.
Yu, X., Wang, J., Liang, J., Li, S., Zeng, X., Li, W., 2014. Depositional characteristics and accumulation model of gas hydrates in northern South China Sea. Mar. Petrol. Geol. 56, 74–86.
Yuan, S., 2009. Sedimentary System of Deepwater Channel, the Slope Area of Northern South China Sea. Insititue of Oceanology, Chinese Academy of Sciences, Qingdao, pp. 1–123.
Zhao, Q., Li, Q., Jian, Z., 2009. Deep waters and oceanic connection. In: Wang, P., Li, Q. (Eds.), The South China Sea. Springer, Netherlands, pp. 395–437.
Zhao, W., Zhou, C., Tian, J., Yang, Q., Wang, B., Xie, L., Qu, T., 2014. Deep water circulation in the Luzon Strait. J. Geophys. Res. Oceans 119, 790–804.
Zhao, Y., Liu, Z., Zhang, Y., Li, J., Wang, M., Wang, W., Xu, J., 2015. In situ observation of contour currents in the northern South China Sea: applications for deepwater sediment transport. Earth Planet Sci. Lett. 430, 477–485.
Zheng, X.D., Zhu, M., He, M., Li, H.W., 2007. Prediction of Liwan deep submarine fan sand body distribution, Baiyun sag, Pearl River Mouth Basin. Petrol. Explor. Dev. 34 (5), 529–533.
Zhu, M., Graham, S., Pang, X., McHargue, T., 2010. Characteristics of migrating submarine canyons from the middle Miocene to present: implications for paleoceanographic circulation, northern South China Sea. Mar. Petrol. Geol. 27 (1), 307–319.
Zhu, W., Huang, B., Mi, L., Wilkins, R.W.T., Fu, N., Xiao, X., 2009. Geochemistry, origin, and deep-water exploration potential of natural gases in the Pearl River Mouth and Qiongdongnan basins, South China Sea. AAPG (Am. Assoc. Pet. Geol.) Bull. 93 (6), 741–761.